Programmed Variations of Cytokinesis Contribute to Morphogenesis in the *C. elegans* embryo

Xiaofei Bai[1], Po-Yi Lee[3], Chin-Yi Chen[3], James R. Simmons[1], Benjamin Nebenfuehr[1,4], Diana Mitchell[1,5], Lindsey R. Klebanow[1,6], Nicholas Mattson[1,7], Christopher Turpin[1], Bi-Chang Chen[2,3], Eric Betzig[2], Joshua N. Bembenek[1*]

[1] Department of Biochemistry, Cellular and Molecular Biology, University of Tennessee, Knoxville, Tennessee, United States of America.
[2]Janelia Research Campus, HHMI, Ashburn, Virginia, United States of America.
[3]Research Center for Applied Science, Academia Sinica, Taiwan.
[4]Current Address: NIDDK, NIH, Bethesda, MD, United States of America.
[5]Current Address: Biological Sciences, University of Idaho, Moscow, Idaho, United States of America.
[6]Current Address: Parker Hannefin Corporation, Macedonia, Ohio, United States of America
[7]Current Address: USFDA/CDER/OPQ/OBP/DBRRI, Silver Springs, MD, United States of America

* Corresponding Author:
Joshua N. Bembenek
1414 Cumberland Ave.
C211 Walters Life Sciences Building
Knoxville, TN 37996
(865)-974-4085
E-mail: bembenek@utk.edu

Abstract

While cytokinesis has been intensely studied, how it is regulated and deployed during development is not well understood, despite a long-standing appreciation that various aspects of cytokinesis vary across cell and tissue types. To address this, we investigated cytokinesis during the invariant lineage of the *C. elegans* embryo. We show that several parameters of cytokinesis are reproducibly altered in different stages of the lineage. During the first two divisions, cells undergo consistent patterns of furrow ingression asymmetry and midbody inheritance, suggesting specific regulation of these events. Later during morphogenesis, in precursor cells of the intestine, pharynx, and amphid sensilla, we find several aspects of cytokinesis are altered including migration of midbodies from their site of formation to the apical surface during cellular polarization. In each case, Aurora B kinase remains associated with the apical membrane after internalization of other midbody components. Perturbations of cytokinesis disrupt lumen formation and dendrite formation. These data reveal that cytokinesis shows surprising diversity during development, and may regulate the final interphase architecture of a terminally dividing cell during morphogenesis.

Introduction

Generation of a multicellular organism requires that carefully orchestrated cell division is integrated properly into different developmental processes. Cell division is required not only to generate new cells that organize into tissues, but also to dictate the size, position and timing of daughter cells that are generated. Several aspects of cell division, including spindle orientation and division symmetry are well known instruments of developmental programs (Siller and Doe, 2009). Roles for cytokinesis in regulating developmental events are emerging, but are much less understood (Chen et al., 2013; Herszterg et al., 2014; Li, 2007). Using live imaging, we sought to investigate cytokinesis using the well-defined divisions of the invariant *C. elegans* embryo lineage, which has been completely described (Sulston et al., 1983).

Cytokinesis is the final step of cell division and is normally a constitutive process during the exit from mitosis defined by discrete steps that occur during "C phase" (Canman et al., 2000; Oegema and Hyman, 2006). During cell division, signals from the anaphase spindle initiate ingression of the cleavage furrow (Bringmann and Hyman, 2005; Eggert et al., 2006), which constricts the plasma membrane onto the spindle midzone and leads to formation of the midbody. The midbody is a membrane channel between daughter cells containing microtubules and a defined organization of more than one hundred proteins that collaborate to execute abscission, the final separation of daughter cells (Green et al., 2012; Hu et al., 2012; Skop et al., 2004). Many of the proteins that contribute to midbody formation and function have roles in the formation of the central spindle and the contractile ring (El Amine et al., 2013). In addition, vesicles are delivered to the midbody that contribute lipids as well as regulators of abscission (Schiel et al., 2013). Subsequently, the ESCRT machinery assembles, microtubules are cleared and membrane scission occurs (Guizetti et al., 2011; Schiel et al., 2011). Aurora B kinase (AIR-2 in *C. elegans*) is required for the completion of cytokinesis, and also regulates the timing of abscission in response to developmental or cell cycle cues partly by regulating the ESCRT machinery (Carlton et al., 2012; Carmena et al., 2015; Mathieu et al., 2013; Norden et al., 2006; Steigemann et al., 2009). Substantial effort has been devoted to understanding factors required to assemble the midbody and the mechanisms of regulation and execution of abscission. In general, while mechanistic details are being elucidated, it is generally assumed that these events occur through a standard, well-defined series of ordered events.

Exceptions to such a clear linear view of cytokinetic events have long been known, but are considered to be specialized cases. The most extreme examples are cells that do not complete cytokinesis altogether and become polyploid, such as liver or intestinal cells (Amini et al., 2015; Fox and Duronio, 2013; Hedgecock and White, 1985; Lacroix and Maddox, 2012). Another well-known example is found in several systems where germ cells do not complete abscission and remain connected through ring canals, which can allow flow of cytoplasm into germ cells (Greenbaum et al., 2007; Haglund et al., 2011; Hime et al., 1996; Maddox et al., 2005). Delayed abscission has also been observed in other cell types to keep daughter cells connected (McLean and Cooley, 2013; Zenker et al., 2017). Other variations of cytokinesis include cleavage furrow re-positioning during anaphase to change the size and fate of daughter cells (Ou et al., 2010). The symmetry of furrow ingression is important in established epithelial tissue where the furrow constricts toward the apical side of the cell and must occur while appropriate cellular contacts are preserved (Herszterg et al., 2014). In zebrafish neuroepithelial divisions, asymmetrical furrowing positions the midbody at the apical domain, which is inherited by the differentiating daughter (Paolini et al., 2015). Therefore, there are a number of ways the standard pattern of cytokinesis can be altered and more investigation is required to understand the functional purpose of these changes and how they are achieved.

Recent studies of abscission have sparked renewed interest in the midbody, which has led to insights into other functions it has beyond abscission (Chen et al., 2013). In general, the midbody is cut off from each of the daughter cells that give rise to it (Crowell et al., 2014; Konig et al., 2017). The midbody may then be engulfed by either cell or persist extracellularly, which can depend on cell type (Ettinger et al., 2011; Salzmann et al., 2014). The midbody can also travel to non-parent cells, suggesting that it may carry or transport signals between cells (Crowell et al., 2014). The midbody is reproducibly inherited in *Drosophila* germline stem cells, but does not always end up in the stem cell (Salzmann et al., 2014). In dividing neuroepithelial cells, a stem cell marker is concentrated at the midbody and released into the lumen of the neural tube, which might provide signals during neuronal development (Dubreuil et al., 2007). This has led to the hypothesis that the midbody provides cues that regulate cell fate, although a detailed mechanistic understanding of this has not been elucidated.

112 A more clearly defined function for the midbody has been uncovered in cells
113 that undergo polarization events after the completion of cytokinesis. For example,
114 Madin-Darby canine kidney (MDCK) cells can establish apical basal polarity and
115 organize into a simple epithelial lumen structure (Reinsch and Karsenti, 1994). Apical
116 membrane markers are first delivered to the midbody during cytokinesis, establishing
117 an apical membrane at the interface between the first two daughter cells (Schluter et
118 al., 2009). Proper abscission and midbody positioning is required, in addition to
119 proper spindle orientation, for MDCK lumen formation (Lujan et al., 2016; Reinsch
120 and Karsenti, 1994). Polarized trafficking during cytokinesis has been shown to
121 promote lumen formation in other systems as well (Wang et al., 2014b). Abscission is
122 also delayed in acentrosomal blastomeres of the early mouse embryo to generate a
123 midzone-derived microtubule organizing center that directs delivery of apical
124 membrane markers to the plasma membrane (Zenker et al., 2017). The midbody
125 becomes the apical process in chick neuronal progenitors (Wilcock et al., 2007) and
126 defines the site of polarization for dendrite extension in *D. melanogaster* neurons
127 (Pollarolo et al., 2011). The midbody is also a polarizing cue in the *C. elegans* embryo
128 during the establishment of dorsoventral axis formation (Singh and Pohl, 2014;
129 Waddle et al., 1994). In addition, the midbody can play a role in cilium formation
130 (Bernabe-Rubio et al., 2016). Further effort is required to understand how cytokinesis
131 and the midbody regulate pattern formation in tissues.
132 In order to further investigate patterns of cytokinesis during development, we
133 examined the invariant *C. elegans* lineage. We find that cytokinesis follows a lineage
134 specific pattern and that furrow symmetry and midbody inheritance is highly
135 reproducible. During morphogenesis, we observe striking midbody migration events
136 in the developing digestive and sensory tissues in *C. elegans*, likely before abscission.
137 Interestingly, AIR-2 migrates with midbodies and remains at several apical surfaces
138 after internalization of different ring components. Coordinated movements of
139 midbodies and differential fates of midbody components are novel behaviors during
140 cytokinesis and are programmed at specific divisions in the embryo. Inactivation of
141 temperature-sensitive midbody proteins disrupt proper formation of several tissues,
142 indicating an important role for specialized cytokinesis during morphogenesis.
143 Together, our results reveal that coordinated alterations in cytokinesis regulation,
144 particularly with regards to the midbody, are critical for proper animal development.

Results

Cytokinesis in the first two mitotic divisions: asymmetric midbody inheritance

We sought to systematically examine cytokinesis using lattice light sheet and spinning disc confocal microscopy during the stereotypical divisions of the *C. elegans* embryo, which has been extensively studied primarily in the first cell division due to its size and ease of access. The first division of the P0 cell generates the larger anterior daughter AB and the posterior daughter P1 (Fig. 1 A). We observed different components that allow us to evaluate specific aspects of the cytokinetic apparatus including the central spindle, the cytokinetic furrow and the midbody. We also chose midbody markers that localize to the flank and ring sub-structures of the midbody (Green et al., 2012). To observe the midbody flank region, we imaged the Aurora B kinase, AIR-2, microtubules, and the membrane trafficking regulator RAB-11 (Fig. 1 and Video S1). We also imaged midbody ring markers including the non-muscle myosin NMY-2 and the centralspindlin component ZEN-4 (Fig. 1 G-P and Video S1). While the first mitotic furrow shows some variable asymmetry as previously demonstrated (Maddox et al., 2007), the midbody forms in a relatively central position between daughter cells (Fig. 1 B-C, G-H and L-M). AIR-2::GFP, endogenous AIR-2 staining and tubulin show the expected pattern of localization on the central spindle and midbody as expected (Fig. 1 B-C, Fig. S1 A-D, Fig. 3 A-B and Video S1). The midbody from the first mitotic division is always inherited by the P1 daughter cell (Fig. 1 A) (Bembenek et al., 2013; Singh and Pohl, 2014). The midbody microtubule signal diminishes within 8 minutes after furrowing onset, which is a general indicator of abscission timing (Fig. 3 B, I) (Green et al., 2013; Konig et al., 2017). AIR-2 is lost from the flank over time but can be observed on the midbody remnant even after it is internalized into P1 (Fig. 1 D-E and Video S1). Additionally, each of the ring components behaves similarly to AIR-2, as expected (Fig. 1 I-J and N-O). Therefore, AIR-2 and other ring components remain co-localized on the midbody throughout the final stages of cytokinesis and are reproducibly internalized by the P1 daughter cell, as previously observed (Bembenek et al., 2013; Ou et al., 2014; Singh and Pohl, 2014).

During the second round of division, we observed substantial, reproducible changes in the pattern of cytokinesis, beginning with furrow symmetry. During the AB daughter cell division, which gives rise to ABa and ABp, the furrow ingressed

178 from the outer surface until it reached the opposite plasma membrane in contact with
179 EMS (Fig. 1 D-E, I-J, N-O). We calculated a symmetry parameter using the ratio of
180 furrow ingression distance from each side of the furrow at completion (Maddox et al.,
181 2007). On average, the furrow symmetry parameter is 1.7 in the first division, while
182 the AB furrow is 21.6 and the P1 furrow is 16.1, indicating highly asymmetric
183 furrows in the second divisions (Fig. 1 V, X). The central spindle is swept from the
184 middle of the AB cell into contact with EMS during furrow ingression (Fig. 1 E,
185 Video S1). AIR-2 localizes to the central spindle, then the midbody flank and remains
186 associated with the midbody remnant after it is engulfed (Fig. 1 D-F, S-U and Video
187 S1). NMY-2 and ZEN-4 also follow the expected pattern during cytokinesis and
188 appear on the midbody that forms in contact with EMS (Fig. 1 I-J, N-O and Video S1).
189 RAB-11::GFP in both the first and second rounds of division accumulates briefly
190 prior to abscission and is not observed on the midbody afterward (Figure 1 Q-U), as
191 shown previously (Ai et al., 2009; Bai and Bembenek, 2017; Bembenek et al., 2010).
192 Therefore, all midbody markers examined behave as expected, localizing to the
193 midbody, which is internalized after abscission is completed.
194 Our examinations of the midbody confirmed the unexpected and consistent
195 pattern of inheritance during the AB division. The midbody from the AB cell division
196 that forms in contact with EMS after highly asymmetric furrowing is invariably
197 engulfed by EMS instead of either of the AB daughter cells (Fig. 1 F, K, P, U, Fig S1
198 D and Video S1). Further, the midbody from the P0 division is also always inherited
199 by EMS. Microtubules in the midbody flank disappear within 8 minutes after
200 furrowing in both AB and P1 cell divisions, indicative of relatively fast abscission at
201 this stage (Fig. 3 C-D and I). Therefore, a consistent pattern of cytokinesis is observed
202 during the first two divisions, involving reproducible furrow ingression symmetry and
203 midbody inheritance. Multiple mechanisms operating during cytokinesis must be
204 properly regulated in order to achieve this highly reproducible pattern. This analysis
205 confirms expected patterns of midbody regulation and midbody protein dynamics
206 during the early embryonic divisions and indicates careful regulation of cytokinesis.
207

208 **Cytokinesis in the intestine epithelia: midbody migration to the apical surface**

209 We next performed a similar analysis of cytokinesis on three developing tissues
210 during morphogenesis, which revealed novel cytokinesis patterns in each. During
211 embryonic morphogenesis, cells undergo terminal divisions and start to form tissues

212 by polarizing and changing shape. The intestine is a well-studied epithelial tube
213 derived from the E blastomere that undergoes five well defined divisions (Leung et al.,
214 1999). The E8 to E16 division occurs around 280 minutes after the first cleavage,
215 after which cells undergo a mesenchyme to epethelial transition involving epithelial
216 polarization and subsequently organize into a tube (Leung et al., 1999). Our
217 observations demonstrate that these cells are performing cytokinesis as they undergo
218 polarization, which to our knowledge has not been previously reported (Fig. 2 A). The
219 E8 cells undergo relatively symmetrical furrowing that produces a centrally placed
220 midbody (Fig. 2 B, E, I, Fig. S2 A and Video S2-4) with a 1.0 symmetry parameter
221 (Fig 1 W, X), in contrast with the highly asymmetric furrow and displaced midbody
222 location during the AB cell division. Therefore, the E8-E16 division appears largely
223 routine up until the point of midbody formation.
224 After midbody formation, there are several changes to the pattern of cytokinesis,
225 which occur as the cells polarize. Using lattice light sheet imaging, we observe that
226 centrally located midbodies from both left and right daughter cell divisions (Ealp,
227 Earp, Epla and Epra) migrate across the width of the cell to the nascent apical surface
228 at the midline, which completes 30 minutes after furrow ingression (Fig. 2 B-D and
229 Video S2). Interestingly, the midbody flank region elongates during the migration
230 process and the flank microtubules persist for over 25 minutes on average from
231 furrow ingression to when they join other microtubules at the apical midline and can
232 no longer be distinguished, which is three times longer than the early divisions (Fig. 3
233 F, H-I). AIR-2::GFP localizes along the extended length of the flank microtubules that
234 move to the apical midline instead of becoming confined to the midbody remnant as
235 observed in early divisions (Fig. 2 E-H, M, and Video S2-4). The ratio of the length of
236 this midbody flank relative to the cell at the greatest length is 0.47 (average 4.6 μm /
237 9.8 μm) in the intestinal cell division, which is more than twice that of the early two
238 cell divisions 0.17 (average 9.3 μm/ 53.4 μm) in P0 and 0.17 (average 7.7 μm/ 44.3
239 μm) in AB (Fig. 2 P-Q). The ring markers ZEN-4 and NMY-2 are quickly
240 internalized (553±140 seconds and 545±179 seconds, respectively) after the midbody
241 reaches the apical midline (Fig. 2 I-L, N-O and Video S3). Collectively, these data
242 indicate that abscission occurs after migration of the midbody to the apical midline.
243 Therefore, E8 cells undergo a novel programmed apical midbody migration event
244 instead of having an asymmetrical furrow lead to the formation of an apically

245 localized midbody, as observed in the AB cell division and epithelial cells in other
246 systems.
247 Next, we noticed that not all midbody components are internalized the end of
248 cytokinesis and some remain on the apical surface. In contrast to the midbody ring
249 components, AIR-2 persists at the apical midline well after the time that ring
250 components are internalized and polarization is complete (Fig. 2 D, G, H, M and
251 Video S2-4), co-localizing with the apical polarity marker PAR-6 (Fig S2 F-H).
252 Endogenous AIR-2 can also be observed at the apical midline by immunofluorescence
253 (Fig. S1 E-G). The gut apical surface recruits pericentriolar material donated by the
254 centrosome during E16 polarization (Feldman and Priess, 2012; Yang and Feldman,
255 2015). We observed that γ-tubulin::GFP moves to the apical surface at the same time
256 as AIR-2::GFP (Fig. S2 I). High temporal resolution single plane confocal imaging to
257 track individual midbody dynamics confirm the elongated AIR-2::GFP flank
258 localization and persistence at the apical midline as well as the rapid internalization of
259 ZEN-4::GFP after the migration event (Fig. 2 M-N and Video S4). Therefore,
260 different midbody components have different fates after cytokinesis in the E8-E16
261 intestinal divisions, with ring markers being internalized while AIR-2 remains at the
262 apical surface. To our knowledge, this is the first report of AIR-2 localization
263 remaining at the plasma membrane after abscission, in most cases it remains on the
264 midbody remnant that is internalized as observed in the early embryo as described
265 above.
266 In other lumen forming systems, such as MDCK cells, RAB-11 vesicle
267 trafficking during cytokinesis transports apical membrane components to the midbody
268 to establish the apical membrane (Schluter et al., 2009). In *C. elegans*, RAB-11
269 endosomes control trafficking at the apical surface of the intestine throughout the life
270 of the animal (Sato et al., 2014). We imaged RAB-11 during the E8-E16 division to
271 examine when apical localization occurs. RAB-11::mCherry colocalizes with AIR-
272 2::GFP once the midbody is formed and migrates to the apical surface with the
273 midbody (Fig. S2 J-L). RAB-11::mCherry is also localized at spindle poles, as in
274 other mitotic cells (Albertson et al., 2005), which also migrate to the apical surface
275 (Feldman and Priess, 2012). Similar to AIR-2, RAB-11 remains localized to the apical
276 surface and appears to remain at this position throughout the life of the animal (Fig.
277 S2 L). These observations indicate that the apical localization of RAB-11 is
278 established during cytokinesis in the E8-E16 division and is delivered at least in part

279 by both the midbody and centrosome. Therefore, cytokinesis is programmed to occur
280 in a specialized way during the E8-E16 division, which may contribute to formation
281 of the apical surface during intestinal epithelial polarization.
282 The anterior and posterior pair of E16 cells (Ealaa, Earaa, Eplpp and Eprpp)
283 undergo one last division to achieve the E20 intestine stage. In the four central E8
284 cells that do not divide again, the midbody migrates to the midline at E8-E16 as
285 described above. However, the midbodies from the other four E8 cells (Eala, Eara,
286 Eplp and Eprp), which undergo another division, migrate toward the midline but the
287 AIR-2 signal diminishes (Fig. S2 E). During the terminal E16-E20 divisions, the
288 midbodies of Ealaa, Earaa, Eplpp and Eprpp undergo apical migration after
289 symmetrical furrowing (Fig. S2 M-O and Video S5). Therefore, the midbody
290 migration event in the intestine does not happen only during the polarization event
291 that occurs during E8-E16, suggesting that it is specifically programmed to occur
292 during the terminal embryonic divisions. It is interesting to note that post-embryonic
293 divisions in the intestine at L1 lethargus involve nuclear but not cytoplasmic divisions
294 leading to the formation of binucleate cells that subsequently undergo multiple rounds
295 of endoreduplication to become highly polyploid (Hedgecock and White, 1985).
296 Therefore, cytokinesis in the intestinal lineage undergoes distinct regulatory phases at
297 different stages of development.
298
299 **Gut lumen formation is disrupted in cytokinesis mutants**
300 Given the pattern of cytokinesis during the E8-E16 division and the localization
301 of AIR-2::GFP to apical structures, we sought to investigate whether cytokinesis is
302 important for lumen formation. First, we assessed whether cytokinesis is essential for
303 embryo viability during later development since it is possible that embryos could still
304 hatch even if terminal divisions fail and morphogenesis occurs with multinucleated
305 cells. To bypass the essential function of cytokinetic regulators during the early
306 embryonic cell divisions, we inactivated temperature sensitive (ts) mutants after
307 isolation of two-cell embryos at the permissive temperature (15 °C) and shifted them
308 to non-permissive temperature (26 °C) at different embryo stages until they hatched.
309 The *air-2 (or207ts)* embryos have only 53.6% (37/69) hatching even when left at
310 15 °C through hatching, indicating that this mutant is sick even at permissive
311 temperature, while wild-type N2, *zen-4 (or153ts)* and *spd-1 (oj5ts)* embryos are 100%
312 viable when kept at 15 °C (Table 1). Embryos shifted to 26 °C after 4.5 hours at 15 °C

313 (corresponding to late E4 to early E8 stages) showed significantly increased lethality
314 in both *air-2(or207ts)* and *zen-4 (or153ts)*, but not *spd-1 (oj5ts)* (Table 1), which
315 correlates with the amount of cytokinesis failure observed. The few animals that were
316 able to hatch in *air-2(or207ts)* and *zen-4 (or153ts)* mutants had severe morphogenesis
317 defects (data not shown). Mutant embryos shifted after the completion of all the
318 developmental divisions at the comma to 1.5-fold stage were largely rescued for
319 lethality and hatched at a rate similar to permissive temperature (Table 1). Therefore,
320 these results are consistent with the hypothesis that cytokinesis is essential for the
321 final stages of embryonic development during morphogenesis.
322 Next, we investigated whether inactivation of cytokinesis mutants late in
323 development affected gut lumen morphogenesis. We evaluated the formation of the
324 apical surface of the intestine by staining for the Ezrin-Radixin-Moesin homologue,
325 ERM-1 (van Furden et al., 2004). The *air-2(or207ts)* mutant fails cytokinesis within
326 minutes after shifting to non-permissive temperature in one-cell embryos (Severson et
327 al., 2000), but does not show penetrant cytokinesis failures unless shifted several
328 hours in older embryos (Figure 4). In comparison, *zen-4 (or153ts)* and *spd-1 (oj5ts)*
329 have similar rapid inactivation kinetics at all stages tested, with *zen-4 (or153ts)*
330 causing penetrant cytokinesis defects while *spd-1 (oj5ts)* does not (data not shown).
331 Therefore, we shifted mutant embryos around the transition between the E4-E8 stages
332 to 26 °C and fixed at the bean stage after intestinal polarization (Fig. 4 A, methods).
333 In all cases, ERM-1 was localized to the apical surface of the intestine and pharynx
334 (Fig. 4 B, Fig. S3 A, D). However, ERM-1 staining was broadened, branched and/or
335 discontinuous in *air-2 (or207ts)* embryos (Fig. 4 C-E, H). Disrupted ERM-1 staining
336 was also observed in *air-2 (or207ts)* embryos, which were shifted at E4-E8 for 4.5-5
337 hours until the comma stage, indicating that these defects are not resolved later in
338 development (Fig. S3 B, D). Furthermore, the intestine was highly mispositioned
339 within the embryo as revealed by color-coded max Z-projections (Figure 4 I) and the
340 nuclei were often randomly positioned on the z-axis compared with wild-type (Fig. 4
341 B, E-F inserts). The localization of other apical markers, such as PAR-3, DLG-1 and
342 IFB-2, were similarly disrupted (Fig. S3 E-J, DLG-1 and IFB-2 data not shown). The
343 *zen-4 (or153ts)* embryos shifted from the E4 stage for 2.5-3 hours until the bean stage
344 also had highly penetrant branched and discontinuous apical ERM-1 staining that was
345 mispositioned within the embryo at a lower rate than the *air-2 (or207ts)* mutants (Fig.
346 4 F, H and Fig. S3 C-D). Interestingly, *spd-1 (oj5ts)* embryos shifted to 26 °C at E4-

347 E8 until the E16-E20 stage displayed a significant, but lower rate of lumen defects
348 (Fig. 4 G-I) despite having no lethality (Table 1) and minimal cytokinesis failures.
349 Therefore, we conclude that proper execution of cytokinesis is required for normal
350 lumen formation in the gut.
351
352 **Cytokinesis in the pharynx: apical midbody migration and AIR-2 accumulation**
353 We also noticed migration of the midbody and accumulation of midbody
354 proteins at the apical surface during the terminal divisions in the pharynx. Unlike the
355 intestine, which originates from a single blastomere that undergoes a very well
356 defined series of divisions, the pharynx has a more complicated structure, containing
357 more than 80 pharyngeal precursor cells (PPCs) that arise from both AB and MS
358 founder cells (Sulston et al., 1983). The PPCs organize into a double plate structure
359 prior to the final division, which occurs at around 310-325 minutes after the first
360 cleavage, and then polarize and undergo apical constriction to become wedge shaped
361 cells that form a lumen by 355 minutes (Rasmussen et al., 2013; Rasmussen et al.,
362 2012). To obtain optimal images of this large, complex structure, we filmed at least a
363 15-micron Z-depth section of the embryo from both dorsal and ventral aspects with
364 confocal microscopy (Figure 5, Video S6). We also filmed whole embryos with lattice
365 light sheet microscopy, which provides higher spatial resolution during the
366 pharyngeal cell division (Video S7). Similar to our observations in the intestine, PPCs
367 are in the final stages of cell division as they polarize, which has not been previously
368 described. PPCs undergo a symmetric furrowing event that yields a centrally placed
369 midbody between the two daughter cells (Fig. 5 A-C, F, G-H, K, L-M, P and Video
370 S6). Also similar to the intestine, PPC midbodies migrate from their central position
371 between daughter cells to the apical midline of the forming pharyngeal bulb (Fig. 5 D,
372 F, I, K, N, P and Video S6). In PPC terminal divisions, AIR-2::GFP appears as a
373 midbody flank structure that migrates to the apical midline and persists at the apical
374 surface after cyst formation (Fig. 5 D, E, F and Video S6). Similar to AIR-2, RAB-11
375 and tubulin accumulate and remain localized to the apical surface after polarization
376 (Fig. S4 A-F). We confirmed this localization with staining and show that endogenous
377 AIR-2 can be observed on the apical surface of the pharynx (Fig. S1 H-J). AIR-2
378 partially co-localized with the apical polarity marker, PAR-6, as well as the
379 centrosome marker γ-tubulin::GFP after polarization (Fig. S4 G-L). ZEN-4::GFP
380 appears on midbodies, migrates to the apical surface, and is rapidly degraded, similar

381 to the intestinal divisions (Fig. 5 J and Video S6). NMY-2::GFP also labels midbodies
382 and moves to the apical surface, but is recruited to the apical surface during apical
383 constriction (Fig. 5 O, P and Video S6) (Rasmussen et al., 2012). Cytokinesis in the
384 gut and pharynx show similar patterns where midbodies migrate to the apical midline
385 and specific midbody components, especially AIR-2, remain localized at the apical
386 cortex even after the midbody ring is removed. Therefore, similar patterns of apical
387 localization and midbody migration are observed during epithelial polarization in the
388 intestine and pharynx in *C. elegans*.
389
390 **Dendrites of sensilla neurons: clustering of midbody components**
391 The *C. elegans* amphid sensilla are a sensory organ that contains 12 neurons
392 with dendrites that extend processes through the cuticle and two sheath cells. During
393 morphogenesis, amphid neurons bundle together, anchor at the tip of the animal and
394 migrate back to extend dendrites (Heiman and Shaham, 2009). From the lineage of
395 the 12 sensilla neurons, there are 10 precursor cell divisions that occur between 280
396 and 400 minutes after the first cleavage (Sulston et al., 1983). These terminal
397 divisions include two daughter cell pairs (ADF/AWB and ASG/AWA) and several
398 where one daughter differentiates into a sensilla neuron while the other daughter
399 undergoes apoptosis (ADL, ASE, ASK, ASI), or differentiates into another neuron
400 (AWC, ASH, AFD, ASJ). Our observations show that these cells undergo a unique
401 form of cytokinesis just before they undergo dendrite morphogenesis (Fig. 6 A).
402 These cells undergo a symmetrical furrowing event before midbodies form centrally
403 between the daughter cells (Fig. 6 B and Video S8-9). A group of at least 6 daughter
404 cell pairs divide initially forming multiple midbodies as observed with both confocal
405 and lattice light sheet imaging (Fig. 6 C and Video S8-9). These midbodies migrate
406 together into a cluster over a 60-minute time window (Fig. 6 D). AIR-2::GFP, RAB-
407 11 and tubulin persist in these clusters (Fig. 6 D, Fig. S5 A-F and Video S8-9), while
408 ZEN-4::GFP rapidly disappears during the midbody clustering process (Fig. 6 E and
409 Video S8). Endogenous AIR-2 can be observed in these lateral apical clusters (Fig. S1
410 K-M). We observe PAR-6 and centrosome marker γ-tubulin::GFP at the tip of the
411 sensilla cluster co-localized with AIR-2, indicating that it is the apical surface of these
412 cells (Fig. 6 G, Fig. S5 G-L). In contrast to ZEN-4::GFP, NMY-2::GFP migrates with
413 the midbody to the cluster and persists at the very tip of the dendrites (Fig. 6 F and

414 Video S8). To our knowledge, this is the first detailed examination of the division and
415 initial steps of organization of these neuronal cell precursors.
416 After formation of the cluster, we observe this apical region move and extend
417 anteriorly until it reaches the tip as the animal progresses from the bean stage through
418 the late comma stage. AIR-2 remains localized along a substantial increasing length
419 of the dendritic extension during the entire elongation process, as does tubulin (Fig. 6
420 H-J, Fig. S5 J-K, M-O and Video S10). As the amphid dendrites extend from the
421 lateral sides of the embryo, other foci of AIR-2 form within the anterior region of the
422 embryo and migrate toward the tip until six sensilla appear at the anterior tip (Fig. 6 J
423 inset, and Video S10). Although the individual cell divisions cannot be easily
424 discerned in this crowded anterior region, these data suggest that the sensilla in the tip
425 of the animal form through a similar process. These results demonstrate that directly
426 after cytokinesis a midbody migration event brings several midbody components to
427 the apical tip of the amphid dendrites, which remain localized there as dendrite
428 extension occurs. Neuronal cell polarization has been suggested to share mechanisms
429 with epithelial morphogenesis (McLachlan and Heiman, 2013), suggesting that these
430 modified cytokinesis events may play a role in cells that undergo epithelial
431 polarization. Therefore, the midbody migrates from its original position at the end of
432 furrowing to the apical surface in several developing tissues during morphogenesis.
433 Interestingly, AIR-2 remains localized at the apical surface of these tissues well after
434 cytokinesis has occurred.
435
436 **Amphid sensilla defects in cytokinesis mutants**
437 Lastly, we investigated whether the developing sensory neurons formed
438 normally in temperature sensitive cytokinesis mutants. *C. elegans* amphid neurons can
439 take up lipophilic dyes such as DiI when they form properly and generate cilia that are
440 exposed to the environment (Hedgecock and White, 1985; Perkins et al., 1986). We
441 maintained embryos at the permissive temperature (15 °C) and shifted them to the
442 non-permissive temperature at different embryo stages until they hatched, then we
443 stained the surviving L1 larvae with DiI. In wild-type, amphid neuron cell bodies,
444 amphid dendrites, and phasmid neurons were clearly labeled by DiI and appeared
445 normal as expected (Fig. 7 A). In the *air-2 (or207ts)* mutant, we observed numerous
446 defects in the subset of surviving embryos that did not fail to hatch and became L1
447 larvae (Fig. 7 B-E). Animals with no observed DiI staining were more common under

448 longer inactivating conditions (Table 2). All *zen-4 (or153ts)* fail to hatch when shifted
449 during E4-E8, preventing analysis of DiI staining (Table 2). When shifted from the E8
450 stage, the few surviving *zen-4 (or153ts)* larvae show severe DiI staining defects,
451 which was dramatically reduced if embryos were shifted after the final divisions at the
452 comma-1.5 fold stage (Fig. 7 F, Table 2). Interestingly, *spd-1 (oj5ts)* animals still had
453 weak defects revealed by DiI staining despite having minimal cytokinesis failures, but
454 never showed a complete lack of staining (Fig. 7I, Table 2). These data are consistent
455 with the hypothesis that proper execution of cytokinesis contributes to proper neurite
456 development. Therefore, cytokinesis and AIR-2 function especially are required late
457 in embryo development for proper morphogenesis of the apical lumen of the gut and
458 proper formation of the sensilla neurons.
459

460 **Discussion**

461 Our results have revealed surprisingly complex and reproducible patterns of
462 cytokinesis during the invariant embryonic divisions in *C. elegans.* The entire
463 invariant lineage has been known for several decades and our results suggest that
464 cytokinesis also follows a specific pattern during the lineage. We observe
465 reproducible alterations to furrow symmetry, central spindle length, abscission timing,
466 midbody movement and inheritance. The traditional view of the embryo lineage is
467 that cells are born and subsequently undergo changes that produce the differentiated
468 organization within a tissue. However, our data demonstrate that cells in multiple
469 tissues are completing cytokinesis when they polarize during morphogenesis, which
470 may impact the regulation of the underlying cellular events. This role for cytokinesis
471 might explain why many cells, including several of the amphid neuronal precursors,
472 divide and produce one daughter cell that undergoes apoptosis instead of finishing the
473 divisions earlier when the right number of cells are generated. A modified cytokinesis
474 in the Q neuroblast generates a smaller daughter cell that undergoes apoptosis, which
475 is prevented if the parameters of cytokinesis change (Ou et al., 2010). Given that the
476 entire cell is reconfigured during mitosis and that cytokinesis is the transition period
477 back into the interphase state, this is an ideal time window to reorganize cellular
478 architecture. Understanding how the developmental plasticity of cytokinesis is
479 regulated will be a fascinating question for future studies.

480 We observe consistent changes to the symmetry of furrow ingression where the
481 first mitosis is relatively symmetric and the second mitosis is highly asymmetric.
482 Previously, the furrow asymmetry in the first division was shown to be a consequence
483 of asymmetric accumulation of contractile ring components during ingression
484 (Maddox et al., 2007). The adhesion between cells may also reinforce this asymmetry
485 to drive the highly asymmetric furrow observed in the second round of divisions
486 (Padmanabhan and Zaidel-Bar, 2017). Whether due to cell intrinsic or extrinsic
487 factors, the asymmetric furrows have previously been postulated to drive efficient
488 furrowing or help maintain proper cell-cell contacts during cytokinesis (Maddox et al.,
489 2007; Morais-de-Sa and Sunkel, 2013). Our data suggest another hypothesis: the
490 asymmetric furrow may be required for the AB midbody to be engulfed by EMS
491 instead of either daughter cell. Given that the midbody has been proposed to deliver
492 signals to cells that inherit it, it is worth noting that the MS cell collects up to four
493 midbodies over time (Singh and Pohl, 2014). Unexpectedly, we see relatively
494 symmetric furrowing in several tissues later in morphogenesis. This is striking
495 because an asymmetric furrow would be sufficient to position the midbody at the
496 nascent apical surface. Given that the polarization mechanisms are not completely
497 understood, for example the extracellular matrix component laminin is required in the
498 pharynx but not the intestine (Rasmussen et al., 2012), the symmetrical furrow
499 followed by midbody migration may be important for defining the apical surface.
500 Perhaps there is no good reference for an asymmetric furrow to position the midbody
501 at the apical surface prior to epithelial polarization in cells in different locations. We
502 hypothesize that lumen formation in the gut and pharynx is analogous to that
503 described in MDCK cells with the formation of a midbody-derived apical-membrane
504 initiation site with the addition of midbody migration for correct positioning of this
505 domain (Li et al., 2014).

506 The coordinated, directed movement of the midbody we observe in several
507 tissues represents a new phenomenon during cytokinesis. Our data also suggest that
508 abscission has not taken place before the midbody migrates in the intestine. This
509 would mean that the two daughter cells polarize while connected at the midbody,
510 which might facilitate their reorganization. These data are somewhat different from
511 what is observed in already polarized epithelia where the furrow constricts from the
512 basal to the apical surface to position the midbody. It is tempting to consider that

513 performing cytokinesis in this particular fashion has an important function in the
514 polarization process. Since these cells are undergoing a mesenchymal to epithelial
515 transition, it is interesting to consider whether cytokinesis may have some general
516 function in executing this process. Previously, midbodies have been shown to
517 reposition after forming under normal or mutant conditions (Bernabe-Rubio et al.,
518 2016; Herszterg et al., 2013; Morais-de-Sa and Sunkel, 2013; Singh and Pohl, 2014),
519 but this phenomena is only appreciated in isolated cases and poorly understood. The
520 entire cortex is controlled by several actin cytoskeletal regulators in order to perform
521 cytokinesis (Jordan and Canman, 2012), perhaps this is also employed to control the
522 movement of the midbody. In the future, it will be important to investigate how the
523 midbody moves to the apical surface after furrowing is completed.

524 In the tissues we investigated, the cells are undergoing their terminal cell
525 division before morphogenesis, although some cells like those in the gut undergo
526 post-embryonic divisions. These cells are also undergoing epithelial polarization and
527 a mesenchymal to epithelial transition. After midbody movement, RAB-11, AIR-2
528 and possibly other molecules are recruited to the apical surface. Certainly, these
529 different tissues have unique gene expression programs, part of which might involve
530 proteins delivered to the midbody and the apical surface. Interestingly, a
531 transmembrane protein that binds to an extracellular partner is expressed in the tip of
532 the dendrites in amphid sensilla, which is required to maintain dendrite attachment at
533 the tip of the embryo (Heiman and Shaham, 2009). It is unknown how this protein
534 localizes to the tip of the dendrite, but one speculative possibility is that it could be
535 delivered through cytokinesis-directed membrane trafficking. A stem cell marker
536 protein is released in extracellular membrane particles by neuroepithelial cells from
537 the cilium and midbody, showing a similarity between these two organelles (Dubreuil
538 et al., 2007). Later in life, the worm releases exosomes from the sensory cilia that
539 form at the tip of the dendrites of the sensilla for communication between animals
540 (Wang et al., 2014a). Perhaps the initial secretory apparatus built during cytokinesis
541 to promote cell division is recruited to the apical surface of these neurons to recruit
542 machinery involved in exosome release. Further investigation is required to define the
543 molecular contributions provided by the midbody to the apical surface of these tissues.
544 Once the midbody moves to the apical surface, we observe that different
545 components of the midbody have different fates. Typically, once the midbody is

546 abscised from the cell, it is thought that most midbody proteins are discarded with the
547 remnant, as observed in the early embryo divisions. Strikingly, we observe Aurora B
548 kinase remaining at the apical surface well after other midbody components like ZEN-
549 4 are removed. The limit of the resolution of light microscopy does not allow us to
550 characterize in detail how this occurs. The most likely model is that the midbody is
551 cut from the plasma membrane and flanking proteins like Aurora B, RAB-11, and
552 microtubules are left behind. Among the many mitotic functions of Aurora B, it is a
553 critical regulator of the timing of abscission (Mathieu et al., 2013; Steigemann et al.,
554 2009). Based on our observations of midbody flank microtubules, abscission may
555 occur after the midbody migration event, and the delay in abscission might require
556 Aurora B activity. Interestingly, inhibition of Aurora B kinase in mouse embryos
557 caused the loss of midbody derived interphase bridges and a reduction of RAB-11 and
558 cell adhesion molecules delivered to apical membranes (Zenker et al., 2017). Aurora
559 B also regulates a number of cytoskeletal regulators during cytokinesis that control
560 cell shape (Ferreira et al., 2013; Floyd et al., 2013; Goto et al., 2003; Kettenbach et al.,
561 2011), and it will be interesting to determine whether any are involved with the events
562 we observed. It is striking that in the intestine, the central spindle elongates
563 dramatically as the midbody migrates, which might also be regulated by Aurora B
564 (Bastos et al., 2013). Along these lines, altered expression of the central spindle
565 protein PRC-1 (the homologue of *spd-1*) contributes to variant midzone microtubule
566 density in different tissues in the *Xenopus* embryo, which correlates with changes to
567 furrow ingression and midbody behavior (Kieserman et al., 2008). While we observe
568 the centralspindlin component ZEN-4 becoming internalized and degraded in the
569 three tissues, it was previously implicated in morphogenesis of the epidermis and
570 pharynx (Hardin et al., 2008; Portereiko et al., 2004; Von Stetina et al., 2017). It
571 remains to be determined whether this role is related to the dynamics of cytokinesis or
572 a cytokinesis-independent function of ZEN-4 as previously suggested. Therefore,
573 further study will be required to understand the role of the central spindle components
574 during the specialized cytokinesis events that occur during morphogenesis.
575 In the sensilla, the centriole moves to the tip of the dendrite to form the base of
576 the sensory cilia of these neurons (Dammermann et al., 2009; Nechipurenko et al.,
577 2017; Perkins et al., 1986). Interestingly, multiple central spindle proteins localize to
578 the base of cilia in *Xenopus* epithelial cells and are required for cilia morphology after
579 the divisions are completed in *C. elegans* (Kieserman et al., 2008; Smith et al., 2011).

580 Additionally, loss of Aurora B kinase causes aberrant neuronal axon morphology, and
581 overexpression of Aurora B causes extended axonal outgrowth in zebrafish (Gwee et
582 al., 2018). At the apical surface of the gut, γ-tubulin and other pericentriolar material
583 is delivered from the centrosome while the centrioles are discarded. The gut apical
584 membrane ultimately becomes elaborated with microvilli (Feldman and Priess, 2012;
585 Leung et al., 1999). We also observed γ-tubulin at the apical surface of the pharynx
586 and sensilla dendrites. Therefore, different material provided by the midbody and
587 centrosome may contribute to the cytoskeletal architecture of the apical surface.
588 Delineating the precise relationship between these two organelles and deciphering
589 how cytokinesis contributes to proper cellular reorganization during morphogenesis
590 will be a major focus of future studies.
591

592 **Acknowledgements**

593 Lattice light sheet microscopy was performed in collaboration with the
594 Advanced Imaging Center at HHMI Janelia Research Campus, a facility jointly
595 supported by the Gordon and Betty Moore Foundation and the Howard Hughes
596 Medical Institute. We appreciate the CGC and Wormbase funded by the NIH Office
597 of Research Infrastructure Programs (P40 OD010440) and National Human Genome
598 Research Institute (U41 HG002223), which provided some *C. elegans* strains and
599 genome information. We are grateful to members of the Bembenek laboratory for
600 productive discussion, reagent preparation and handling strains. We also thank Dr.
601 Max Heiman, Dr. Zhirong Bao for discussions and Dr. Don Fox, Dr. John White, Dr.
602 John Heddleston, Dr. Heidi Hehnley-Chang, Lindsay Rathbun, and Erica Colicino for
603 critical feedback on the manuscript.

604 **Figure Legends**

605 **Figure 1. Cytokinesis in the first two mitotic divisions**

606 (A) Illustration of cytokinesis in the first two mitotic divisions indicating the invariant fate of
607 the midbody after division. Orange arrowheads indicate the first midbody, while blue
608 arrowheads indicate the AB midbody. (B-F) Cytokinesis labeled with AIR-2::GFP (green)
609 and PH::mCherry (magenta), H2B::mCherry (magenta). During late anaphase, Aurora B
610 localizes on the central spindle (B) which condenses into the midbody flank (C, white arrow
611 head) and remains on the midbody until it is internalized by the AB daughter cell (D, white
612 arrowhead). During the second mitosis, the furrow is highly asymmetric and sweeps the
613 central spindle against the EMS boundary, where the midbody forms (E, red arrowhead).
614 EMS engulfs the midbody instead of either of the AB daughter cells (F, red arrowhead). (G-K)
615 NMY-2::GFP (green) and PH::mCherry (magenta) show localization to the furrow (G) and
616 midbody ring (H-K, white arrowhead indicates first midbody, red arrowhead indicates AB
617 midbody). (L-P) ZEN-4::GFP (green) appears on the central spindle (L) and the midbody (M-
618 P white arrowhead indicates first midbody, red arrowhead indicates AB midbody). (Q-U)
619 RAB-11::mCherry (green) co-localized with AIR-2::GFP (magenta) briefly at the midbody,
620 but does not remain on the midbody once it is internalized into cytosol (R-U). (V-X)
621 Quantification of furrow asymmetry, measurement illustrated in V, W. (X) Asymmetry
622 parameter is significantly greater in second cell division. Scale bar, 10 μm.

623

624 **Figure 2. Cytokinesis in the E8-E16 intestinal divisions**

625 (A) Diagram of cytokinesis in the intestinal E8-E16 mitotic divisions depicting midbody
626 dynamics (ring components, red; flank region, green). (B-D) Lattice light sheet imaging of
627 E8-E16 intestinal cell divisions in embryos expressing AIR-2::GFP (green) with
628 PH::mCherry (magenta). AIR-2::GFP labels midbodies (labeled 1-8 in B) in the middle of
629 daughter cell pairs, which migrate (arrowheads, C) to the nascent apical membrane where it
630 persists well after polarization is complete (time shown in minutes:seconds bottom left). (E-G)
631 Spinning disc confocal microscopy of AIR-2::GFP (green) with H2B::mCherry (magenta)
632 and PH::mCherry, (magenta, time shown in minutes:seconds bottom left). (H) Image series of
633 Epla division with AIR-2::GFP (green, PH::mCherry, magenta) starting in prometaphase,
634 clearly indicating midbody formation and migration to apical midline. (I-K) NMY-2 (green)
635 localizes to furrows, then midbody rings (labeled 1-8 in F) that move to the midline
636 (arrowheads, J) but do not persist (rectangle box in K). (L) Montage showing a single NMY-
637 2::GFP labeled midbody migrating to midline. (M-N) Single plane imaging of midbody
638 dynamics in individual intestine cell shows growth of the central spindle with AIR-2::GFP (M)

639 and rapid internalization of ZEN-4::GFP to the cytosol (time in minute: second indicated on
640 right top). (O) Quantification of midline perdurance of different midbody components
641 (measured from the end of furrowing to internalization or loss of signal). (P) Illustration of E8
642 division and (Q) quantification of the ratio of maximal midbody flank length to cell length.
643 Scale bar, 10 μm. Error bars indicate standard deviation of the mean.

644

645 **Figure 3. Comparison of central spindle microtubule dynamics**

646 Imaging of microtubule dynamics during different cell divisions to visualize central spindle
647 and midbody flank microtubules. (A-B) AIR-2::GFP (magenta) and β-tubulin TBB-
648 1::mCherry (green) colocalize at the central spindle during anaphase and furrowing in the first
649 cell division. AIR-2::GFP persists at the midbody after microtubules are lost, which correlates
650 closely with abscission timing (B). (C-D) AIR-2::GFP (magenta) and β-tubulin TBB-
651 1::mCherry (green) colocalize on the central spindle adjacent to EMS after highly asymmetric
652 furrowing. Microtubules are lost in a similar amount of time as the first division (D). (E-G)
653 Tubulin TBB-1::mCherry (green) and AIR-2::GFP (magenta) localize to an extended flank
654 region during intestinal midbody migration (F, arrowheads). (G) Tubulin and AIR-2 persist at
655 the apical membrane after polarization (rectangle box). (H) Single z-plane imaging of
656 midbody flank microtubules (arrowheads) from the dorsal aspect during Epra cell division
657 and midbody migration. The extended flanking microtubules persist at least 3 times longer
658 than earlier divisions throughout the migration process until they can no longer be
659 distinguished from other microtubules at the apical surface. (I) Quantification of tubulin
660 persistence time at the central spindle during different cell divisions. Scale bar, 10 μm. Error
661 bars indicated standard deviation of the mean.

662

663 **Figure 4**. **Cytokinesis mutants have disrupted intestinal morphogenesis**

664 Shifting temperature-sensitive cytokinesis mutants to 25 °C at the E4-E8 stage until they
665 reach the bean stage causes severe lumen defects in the intestine. (A) Timeline of cell division
666 events in the intestine emphasizing E4-E8 timing and E8-E16 cytokinesis and the timing of
667 temperature shift experiments. (B) ERM-1 staining in wild type bean stage embryos is
668 enriched at the apical midline of the intestine (dotted rectangle). Maximum z-projected
669 images color-coded according to Z-depth (using FIJI temporal-color code plugin, scale shown
670 in I) to visualize the three-dimensional position of ERM-1 and nuclei (B-G, I). In *air-*
671 *2(or207ts)*, multiple defects are observed, including mispositioning of the entire intestine (C-
672 E), branches in the apical surface (C), gaps in the apical surface creating a discontinuous

673 lumen (D), or broader staining of ERM-1 (E). (F) The *zen-4(or153ts)* mutant causes many of
674 these phenotypes, including branching of the apical surface. (G) There are subtle lumen and
675 nuclei position defects in *spd-1(oj5ts)* embryos. (H) Quantification of apical defects observed
676 by ERM-1 staining in the different mutants. (I) Quantification of the defective z-plane
677 distribution of the apical surface in the different mutants. The more colors a lumen has in the
678 projection, the more skewed in the Z-axis it is within the embryo. Scale bar, 10 µm.

679

680 **Figure 5. Cytokinesis During Pharyngeal Precursor Cell Polarization**

681 (A) Illustration of the mesenchymal to epithelial transition of pharyngeal precursor cells
682 (PPCs) showing cell division and dynamics of Aurora B (green, midbody ring in red). (B-E)
683 PPC division labeled with AIR-2::GFP (green, H2B::mCherry in magenta) from both ventral
684 (B-D) and dorsal (E) views. AIR-2::GFP localizes to chromatin in metaphase (B) and moves
685 to the central spindle in anaphase (C) and appears on the midbody which moves toward the
686 midline (D). AIR-2 persists at the apical surface for an extended time (E, time in
687 minutes:seconds indicated below). (F) Image series showing an AIR-2::GFP labeled midbody
688 migrating toward the midline. Imaging two different midbody ring components, (G-K) ZEN-4
689 (green, TBB-1::mCherry in magenta) and (L-P) NMY-2 (green, TBB-1::mCherry in magenta),
690 shows the movement of the midbody to the midline (I, N). ZEN-4 does not persist (J, arrows
691 indicate internalized midbodies not yet degraded), while NMY-2 accumulates at the apical
692 midline during apical constriction (O). Time shown in minutes: seconds. Scale bar, 10 µm.

693

694 **Figure 6**. **Midbody components label dendrites of sensilla neurons**

695 (A) Diagram of sensilla precursor cell (SPC) divisions and the localization of apical midbody
696 components during the initial events of polarization. (B-D) Cytokinesis in SPCs in the
697 anterior lateral region of the embryo expressing AIR-2::GFP (green, H2B::Cherry in magenta)
698 gives rise to multiple midbodies (arrowheads B,C) that cluster together at the lateral sides of
699 the embryos (D). (E) The midbody ring marker ZEN-4::GFP (green, microtubules in magenta)
700 is internalized and degraded before the cluster forms, which is also concentrated with
701 microtubules (arrowheads). (F) NMY-2::GFP (green, microtubules in magenta) localizes to
702 midbodies that cluster and remain at the tip as the dendrite extension forms. (G) PAR-
703 6::mCherry (green, AIR-2::GFP in magenta) localizes to tip of the cluster (arrowheads) and
704 persists at the tip of the dendrites as they extend, indicating that this is the apical surface of
705 these cells. (H-J) After the apical surface cluster forms, AIR-2::GFP remains at the tip (red
706 arrowheads) as the cells migrate to the nose of the animal. AIR-2::GFP also labels a

707 substantial portion of the length of the dendrite as they extend (J). Insert in (J) is a rotated
708 max z-projection showing the anterior end of the animal after multiple sensilla form (J). Time
709 shown in minutes:seconds. Scale bar, 10 μm.

710

711 **Figure 7**. **Cytokinesis mutants have disrupted sensilla neuron morphogenesis**

712 (A-E) Visualizing dendrite and neuron morphology by DiI staining in surviving larvae after
713 shifting mutants to 25 °C at the E4 or E8 stage until hatching. (A) In wild type animals, two
714 dendrite bundles can be clearly observed as well as amphid and phasmid neurons. (B-E)
715 Hatched mutant larvae displayed a variety of neurite defects, including No-DiI signal (B, F),
716 Weak signal (C, G), dendrite shape and positioning defects (D) and additional diffuse staining
717 throughout the head of the animal (E, H, I).
718

719 **Materials and Methods**

720 ***C. elegans* Strains**

721 *C. elegans* strains were maintained with standard protocols. *C. elegans* strains
722 expressing midbody proteins driven by the *pie-1* promoter are listed in Table 2. All
723 temperature-sensitive mutants were obtained from the Caenorhabditis Genetics Center.
724

725 **Embryo Preparation and Imaging**

726 For live imaging, young gravid hermaphrodites were dissected in M9 buffer
727 containing polystyrene microspheres and sealed between two coverslips with vaseline
728 (Pohl and Bao, 2010). Live cell imaging was performed on a spinning disk confocal
729 system that uses a Nikon Eclipse inverted microscope with a 60 X 1.40NA objective,
730 a CSU-22 spinning disc system, and a Photometrics EM-CCD camera from Visitech
731 International. Images were acquired by Metamorph (Molecular Devices) and analyzed
732 by ImageJ/FIJI Bio-Formats plugins (National Institutes of Health) (Linkert et al.,
733 2010; Schindelin et al., 2012). Whole embryo live imaging was performed on a lattice
734 light sheet microscopes housed in the Eric Betzig lab, Bi-Chang Chen lab, or the
735 Advanced Imaging Center at HHMI Janelia. The system is configured and operated as
736 previously described (Chen et al., 2014). Briefly, embryos were dissected out and
737 adhered to 5 mm round glass coverslips (Warner Instruments, Catalog # CS-5R).
738 Samples were illuminated by lattice light-sheet using 488 nm or 560 nm diode lasers
739 (MPB Communications) through an excitation objective (Special Optics, 0.65 NA,
740 3.74-mm WD). Fluorescent emission was collected by detection objective (Nikon,
741 CFI Apo LWD 25XW, 1.1 NA), and detected by a sCMOS camera (Hamamatsu Orca
742 Flash 4.0 v2). Acquired data were deskewed as previously described (Chen et al.,
743 2014) and deconvolved using an iterative Richardson-Lucy algorithm. Point-spread
744 functions for deconvolution were experimentally measured using 200nm tetraspeck
745 beads adhered to 5 mm glass coverslips (Invitrogen, Catalog # T7280) for each
746 excitation wavelength.
747

748 **Immunostaining Assay in *C. elegans* Embryos**

749 Apical marker staining was performed with the freeze-crack methanol protocol
750 (Leung et al., 1999). Immunostaining with anti-AIR-2 antibodies was performed as
751 described (Schumacher et al., 1998). Primary antibodies and (dilutions) used were
752 anti-ERM-1 (1:200); P4A1/PAR-3 (1:200); DLG-1 (1:200); MH33 (1:150); AIR-2

753 (1:50). 1:200-400 dilutions of Alexa 588 and 468 secondary antibodies were used in
754 the study. To stain temperature-sensitive mutants, two-cell stage embryos were
755 dissected from gravid worms, mounted in 10 μL of M9 buffer, and kept cold on ice.
756 The two-cell stage embryos were incubated at 15 °C for 4-7 hours until specific stages,
757 then shifted to the restrictive temperature (25 °C) for 2-4 hours and stained as
758 described above.
759
760 **DiI staining in *C. elegans***
761 DiI staining of wild-type and temperature sensitive mutants was done as previously
762 described (Tong and Burglin, 2010). Two-cell stage embryos were incubated at 15 °C
763 for 6.5~7 hours until they reached the polarized E16 stage, then shifted to the
764 restrictive temperature (25 °C) with 1:200 dilution of stock DiI dye solution
765 containing 2 mg/mL DiI in dimethyl formamide for 18-24 hours. Hatched larvae were
766 transferred to M9 and washed twice in M9 before mounting in 25 mM levamisole on
767 2% agar pads for imaging.
768
769 **Temperature-Shift Experiments**
770 Temperature-sensitive mutants were maintained at 15 °C. To perform temperature
771 shifts on staged embryos, gravid adults were transferred to a dissection chamber (<
772 4 °C), which was precooled in ice bucket, with 20 μL of ice-cold M9 Buffer. Two-
773 Cell stage embryos were quickly transferred (within a 5-10 minute time window) via
774 mouth pipette (Aspirator tube assemblies, Sigma) to Fisherbrand Hanging Drop Slides
775 (Catalogue #12-560B) on ice. The slide was placed into a humidified chamber and
776 incubated at 15 °C until the appropriate stages were reached and then shifted to 26 °C.
777 Incubation times were determined based on *C. elegans* embryonic lineage timing and
778 adjusted according to DAPI staining to ensure each mutant was shifted at a similar
779 stage of embryo development. To inactivate *air-2 (or207ts)*, mutant embryos were
780 incubated for 5 hours at 15 °C and shifted to 26 °C for 3 hours to reach the bean stage
781 or 5 hours at 26 °C to reach the comma stage. This was the minimum amount of time
782 to shift embryos to non-permissive temperature and observe significant cytokinesis
783 defects by the E8-E16 division, indicating significant reduction of AIR-2 function.
784 Most embryos reached the E4-E8 division at the time of the shift. By live imaging we
785 found that there was little disruption of the E4-E8 division under these conditions

786 since (n=4/5) *air-2 (or207ts)* embryos have 8 normal E8 cells. N2*, spd-1 (oj5ts)*, and
787 *zen-4 (or153ts)* embryos were incubated for 4.5 hours at 15 °C to reach E4-E8 stage,
788 followed by 3 hours at 26 °C to reach the bean stage and 5 hours at 26 °C to reach the
789 comma stage. To shift embryos at the comma stage*, air-2 (or207ts)* embryos were
790 incubated for 12 hours at 15 °C and N2*, spd-1 (oj5ts) and zen-4 (or153ts)* embryos
791 were incubated 11-11.5 hours at 15 °C.

792

793

794

795 **Table 1. Hatch rate of temperature sensitive mutants.**

796

Stage Before Shifting	Genotype	Hatch Rate % (Hatch Embryos/Total)
15 °C Forever	N2	100% (32/32)
	air-2 (or207ts)	53.6% (37/69)
	zen-4 (or153ts)	100% (28/28)
	spd- (oj5ts)	100% (35/35)
E4-E8	N2	100% (26/26)
	air-2 (or207ts)	6.3% (2/32)
	zen-4 (or153ts)	0% (0/57)
	spd- (oj5ts)	100% (48/48)
E8-E16	N2	100% (45/45)
	air-2 (or207ts)	14.4% (13/90)
	zen-4 (or153ts)	10.1% (10/99)
	spd- (oj5ts)	100% (83/83)
Comma-1.5 Fold	N2	100% (36/36)
	air-2 (or207ts)	33.7% (31/92)
	zen-4 (or153ts)	85.7% (54/63)
	spd- (oj5ts)	100% (27/27)

797

Table 2. Quantification of DiI Staining of Temperature-Sensitive Mutants

Stage Before Shifting	Genotype	No DiI Signal	Weak DiI signal	Shape & Position Defect	Extended DiI Staining
15 °C Forever	N2	0% (0/32)	0% (0/32)	0% (0/32)	0% (0/32)
	air-2(or207ts)	2.7% (1/37)	8.1% (3/37)	2.7% (1/37)	0% (0/37)
	zen-4(or153ts)	0% (0/18)	0% (0/18)	0% (0/18)	0% (0/18)
	spd-1(oj5ts)	0% (0/34)	0% (0/34)	0% (0/34)	0% (0/34)
E4-E8	N2	0% (0/10)	0% (0/10)	0% (0/10)	0% (0/10)
	air-2(or207ts)	50% (1/2)	0% (0/2)	50% (1/2)	0% (0/2)
	zen-4(or153ts)	0% (0/0)	0% (0/0)	0% (0/0)	0% (0/0)
	spd-1(oj5ts)	0% (0/44)	4.5% (2/44)	9.1% (4/44)	6.8% (3/44)
E8-E16	N2	0% (0/29)	0% (0/29)	0% (0/29)	0% (0/29)
	air-2(or207ts)	16.7% (2/12)	58.3% (7/12)	58.3% (7/12)	0% (0/12)
	zen-4(or153ts)	77.8% (7/9)	11.1% (1/9)	22.2% (2/9)	0% (0/9)
	spd-1(oj5ts)	0% (0/59)	0% (0/59)	8.5% (5/59)	5.1% (3/59)
Comma-1.5 Fold	N2	0% (0/21)	0% (0/21)	0% (0/21)	0% (0/21)
	air-2(or207ts)	6.9% (2/29)	10.3% (3/29)	0% (0/29)	13.8% (4/29)
	zen-4(or153ts)	0% (0/53)	0% (0/53)	0% (0/53)	22.6% (12/53)
	spd-1(oj5ts)	0% (0/18)	0% (0/18)	0% (0/18)	33.3% (6/18)

800 **Table 3. Strains used in this study.**

Strain	**Genotype**
N2	Bristol (wild-type)
EKM48	*unc-119(ed3) iii; ojIs51 [Ppie-1::GFP::air-2; unc-119(+)]*
EKM50	*unc-119(ed3) iii; ojIs51 [Ppie-1::GFP::air-2; unc-119(+)]; ItIs37 [Ppie-1::mCherry::his-58 (pAA64); unc-119(+)] iv; ItIs44 [Ppie-1::mCherry::PH (PLC1delta1); unc-119(+)]v*
EKM51	*unc-119(ed3) iii; ojIs51 [Ppie-1::GFP::air-2; unc-119(+)]; ItIs37 [Ppie-1::mCherry::his-58 (pAA64); unc-119(+)] iv*
EKM52	*unc-119(ed3) iii; ojIs51 [Ppie-1::GFP::air-2; unc-119(+)]; ItIs44 [Ppie-1::mCherry::PH (PLC1delta1); unc-119(+)] v*
JAB23	*unc-119(ed3) iii; ojIs51 [Ppie-1::GFP::air-2; unc-119(+)]; weIs21 [pJA138 (pie-1::mCherry::tub)]*
JAB60	*unc-119(ed3) iii; ojIs51 [Ppie-1::GFP::air-2; unc-119(+)]; pwIs476 [Ppie-1::mCherry::rab-11]*
JAB116	*unc-119(ed3) iii; weIs21 [pJA138 (Ppie-1::mCherry::tub)]; unc-119(+)]; zuIs45 [nmy-2::NMY-2::GFP; unc-119(+)] v*
NWG002	*unc-119(ed3) iii; ItIs44 [Ppie-1::mCherry::PH (PLC1delta1); unc-119(+)]v; zuIs45 [nmy-2::NMY-2::GFP; unc-119(+)] v*
JAB24	*zen-4(or153ts) iv; xsEx6 [zen-4::GFP; rol-6 (su1006)]; unc-119(ed3) iii; weIs21 [pJA138 (pie-1::mCherry::tub)]*
JAB34	*zen-4(or153) iv; xsEx6 [zen-4::GFP; rol-6 (su1006)]; unc-119(ed3) iii; ItIs44 [Ppie-1::mCherry::PH (PLC1delta1); unc-119(+)] v*
JAB32	*unc-119(ed3) iii; ddIs26 [Ppie-1::mCherry::T26E3.3; unc-119(+)]v; ojIs51 [Ppie-1::GFP::air-2; unc-119(+)]*
EU630	*air-2(or207) i.*
EU716	*zen-4(or153) iv.*

WH12	*spd-1 (oj5) i.*
WH421	*unc-119(ed3) iii; ojIs51 [Ppie-1::GFP::air-2; unc-119(+)];spd-1 (oj5) i.*
JAB39	*unc-119(ed3) iii; ruls32III;dd156[tbg-1::GFP;unc-119(+)];; ojIs51 [Ppie-1::GFP::air-2; unc-119(+)];spd-1 (oj5) i.*
JAB52	*unc-119(ed3) iii; ruls32III;dd156[tbg-1::GFP;unc-119(+)]; ruls32[Ppi-1::GFP::His-58; unc-119(ed3); weIs21 [pJA138 (pie-1::mCherry::tub)]*

801

802 Bibliography

803 Ai, E., Poole, D.S., and Skop, A.R. (2009). Rack-1 Directs Dynactin-dependent RAB-11
804 Endosomal Recycling during Mitosis in Caenorhabditis elegans (vol 20, 1629, 2009). Mol
805 Biol Cell *20*, 5036-5036.
806 Albertson, R., Riggs, B., and Sullivan, W. (2005). Membrane traffic: a driving force in
807 cytokinesis. Trends Cell Biol *15*, 92-101.
808 Amini, R., Goupil, E., Labella, S., Zetka, M., Maddox, A.S., Labbe, J.C., and Chartier, N.T.
809 (2015). C. elegans Anillin proteins regulate intercellular bridge stability and germline
810 syncytial organization (vol 206, pg 129, 2014). J Cell Biol *209*, 467-467.
811 Bai, X.F., and Bembenek, J.N. (2017). Protease dead separase inhibits chromosome
812 segregation and RAB-11 vesicle trafficking. Cell Cycle *16*, 1902-1917.
813 Bastos, R.N., Gandhi, S.R., Baron, R.D., Gruneberg, U., Nigg, E.A., and Barr, F.A. (2013).
814 Aurora B suppresses microtubule dynamics and limits central spindle size by locally
815 activating KIF4A. J Cell Biol *202*, 605-621.
816 Bembenek, J.N., Verbrugghe, K.J.C., Khanikar, J., Csankovszki, G., and Chan, R.C. (2013).
817 Condensin and the Spindle Midzone Prevent Cytokinesis Failure Induced by Chromatin
818 Bridges in C. elegans Embryos. Curr Biol *23*, 937-946.
819 Bembenek, J.N., White, J.G., and Zheng, Y.X. (2010). A Role for Separase in the Regulation
820 of RAB-11-Positive Vesicles at the Cleavage Furrow and Midbody. Curr Biol *20*, 259-264.
821 Bernabe-Rubio, M., Andres, G., Casares-Arias, J., Fernandez-Barrera, J., Rangel, L., Reglero-
822 Real, N., Gershlick, D.C., Fernandez, J.J., Millan, J., Correas, I.*, et al.* (2016). Novel role for
823 the midbody in primary ciliogenesis by polarized epithelial cells. J Cell Biol *214*, 259-273.
824 Bringmann, H., and Hyman, A.A. (2005). A cytokinesis furrow is positioned by two
825 consecutive signals. Nature *436*, 731-734.
826 Canman, J.C., Hoffman, D.B., and Salmon, E.D. (2000). The role of pre- and post-anaphase
827 microtubules in the cytokinesis phase of the cell cycle. Curr Biol *10*, 611-614.
828 Carlton, J.G., Caballe, A., Agromayor, M., Kloc, M., and Martin-Serrano, J. (2012). ESCRT-
829 III Governs the Aurora B-Mediated Abscission Checkpoint Through CHMP4C. Science *336*,
830 220-225.
831 Carmena, M., Earnshaw, W.C., and Glover, D.M. (2015). The Dawn of Aurora Kinase
832 Research: From Fly Genetics to the Clinic. Front Cell Dev Biol *3*, 73.
833 Chen, B.C., Legant, W.R., Wang, K., Shao, L., Milkie, D.E., Davidson, M.W., Janetopoulos,
834 C., Wu, X.F.S., Hammer, J.A., Liu, Z.*, et al.* (2014). Lattice light-sheet microscopy: Imaging
835 molecules to embryos at high spatiotemporal resolution. Science *346*, 439-+.
836 Chen, C.T., Ettinger, A.W., Huttner, W.B., and Doxsey, S.J. (2013). Resurrecting remnants:
837 the lives of post-mitotic midbodies. Trends Cell Biol *23*, 118-128.
838 Crowell, E.F., Gaffuri, A.L., Gayraud-Morel, B., Tajbakhsh, S., and Echard, A. (2014).
839 Engulfment of the midbody remnant after cytokinesis in mammalian cells. J Cell Sci *127*,
840 3840-3851.
841 Dammermann, A., Pemble, H., Mitchell, B.J., McLeod, I., Yates, J.R., Kintner, C., Desai,
842 A.B., and Oegema, K. (2009). The hydrolethalus syndrome protein HYLS-1 links core
843 centriole structure to cilia formation. Gene Dev *23*, 2046-2059.
844 Dubreuil, V., Marzesco, A.M., Corbeil, D., Huttner, W.B., and Wilsch-Brauninger, M. (2007).
845 Midbody and primary cilium of neural progenitors release extracellular membrane particles
846 enriched in the stem cell marker prominin-1. J Cell Biol *176*, 483-495.
847 Eggert, U.S., Mitchison, T.J., and Field, C.M. (2006). Animal cytokinesis: From parts list to
848 mechanisms. Annu Rev Biochem *75*, 543-566.
849 El Amine, N., Kechad, A., Jananji, S., and Hickson, G.R. (2013). Opposing actions of septins
850 and Sticky on Anillin promote the transition from contractile to midbody ring. J Cell Biol *203*,
851 487-504.
852 Ettinger, A.W., Wilsch-Brauninger, M., Marzesco, A.M., Bickle, M., Lohmann, A., Maliga,
853 Z., Karbanova, J., Corbeil, D., Hyman, A.A., and Huttner, W.B. (2011). Proliferating versus

854 differentiating stem and cancer cells exhibit distinct midbody-release behaviour. Nat
855 Commun *2*, 503.
856 Feldman, J.L., and Priess, J.R. (2012). A role for the centrosome and PAR-3 in the hand-off
857 of MTOC function during epithelial polarization. Curr Biol *22*, 575-582.
858 Ferreira, J.G., Pereira, A.J., Akhmanova, A., and Maiato, H. (2013). Aurora B spatially
859 regulates EB3 phosphorylation to coordinate daughter cell adhesion with cytokinesis. J Cell
860 Biol *201*, 709-724.
861 Floyd, S., Whiffin, N., Gavilan, M.P., Kutscheidt, S., De Luca, M., Marcozzi, C., Min, M.,
862 Watkins, J., Chung, K., Fackler, O.T.*, et al.* (2013). Spatiotemporal organization of Aurora-B
863 by APC/CCdh1 after mitosis coordinates cell spreading through FHOD1. J Cell Sci *126*,
864 2845-2856.
865 Fox, D.T., and Duronio, R.J. (2013). Endoreplication and polyploidy: insights into
866 development and disease. Development *140*, 3-12.
867 Goto, H., Yasui, Y., Kawajiri, A., Nigg, E.A., Terada, Y., Tatsuka, M., Nagata, K., and
868 Inagaki, M. (2003). Aurora-B regulates the cleavage furrow-specific vimentin
869 phosphorylation in the cytokinetic process. J Biol Chem *278*, 8526-8530.
870 Green, R.A., Mayers, J.R., Wang, S., Lewellyn, L., Desai, A., Audhya, A., and Oegema, K.
871 (2013). The midbody ring scaffolds the abscission machinery in the absence of midbody
872 microtubules. J Cell Biol *203*, 505-520.
873 Green, R.A., Paluch, E., and Oegema, K. (2012). Cytokinesis in Animal Cells. Annu Rev Cell
874 Dev Bi *28*, 29-+.
875 Greenbaum, M.P., Ma, L., and Matzuk, M.M. (2007). Conversion of midbodies into germ cell
876 intercellular bridges. Developmental Biology *305*, 389-396.
877 Guizetti, J., Schermelleh, L., Mantler, J., Maar, S., Poser, I., Leonhardt, H., Muller-Reichert,
878 T., and Gerlich, D.W. (2011). Cortical constriction during abscission involves helices of
879 ESCRT-III-dependent filaments. Science *331*, 1616-1620.
880 Gwee, S.S.L., Radford, R.A.W., Chow, S., Syal, M.D., Morsch, M., Formella, I., Lee, A.,
881 Don, E.K., Badrock, A.P., Cole, N.J.*, et al.* (2018). Aurora kinase B regulates axonal
882 outgrowth and regeneration in the spinal motor neurons of developing zebrafish. Cell Mol
883 Life Sci.
884 Haglund, K., Nezis, I.P., and Stenmark, H. (2011). Structure and functions of stable
885 intercellular bridges formed by incomplete cytokinesis during development. Commun Integr
886 Biol *4*, 1-9.
887 Hardin, J., King, R., Thomas-Virnig, C., and Raich, W.B. (2008). Zygotic loss of ZEN-
888 4/MKLP1 results in disruption of epidermal morphogenesis in the C. elegans embryo. Dev
889 Dyn *237*, 830-836.
890 Hedgecock, E.M., and White, J.G. (1985). Polyploid Tissues in the Nematode
891 Caenorhabditis-Elegans. Developmental Biology *107*, 128-133.
892 Heiman, M.G., and Shaham, S. (2009). DEX-1 and DYF-7 establish sensory dendrite length
893 by anchoring dendritic tips during cell migration. Cell *137*, 344-355.
894 Herszterg, S., Leibfried, A., Bosveld, F., Martin, C., and Bellaiche, Y. (2013). Interplay
895 between the Dividing Cell and Its Neighbors Regulates Adherens Junction Formation during
896 Cytokinesis in Epithelial Tissue. Dev Cell *24*, 256-270.
897 Herszterg, S., Pinheiro, D., and Bellaiche, Y. (2014). A multicellular view of cytokinesis in
898 epithelial tissue. Trends Cell Biol *24*, 285-293.
899 Hime, G.R., Brill, J.A., and Fuller, M.T. (1996). Assembly of ring canals in the male germ
900 line from structural components of the contractile ring. Journal of Cell Science *109*, 2779-
901 2788.
902 Hu, C.K., Coughlin, M., and Mitchison, T.J. (2012). Midbody assembly and its regulation
903 during cytokinesis. Mol Biol Cell *23*, 1024-1034.
904 Jordan, S.N., and Canman, J.C. (2012). Rho GTPases in Animal Cell Cytokinesis: An
905 Occupation by the One Percent. Cytoskeleton *69*, 919-930.
906 Kettenbach, A.N., Schweppe, D.K., Faherty, B.K., Pechenick, D., Pletnev, A.A., and Gerber,
907 S.A. (2011). Quantitative Phosphoproteomics Identifies Substrates and Functional Modules of
908 Aurora and Polo-Like Kinase Activities in Mitotic Cells. Sci Signal *4*.

Kieserman, E.K., Glotzer, M., and Wallingford, J.B. (2008). Developmental regulation of central spindle assembly and cytokinesis during vertebrate embryogenesis. Curr Biol *18*, 116-123.
Konig, J., Frankel, E.B., Audhya, A., and Muller-Reichert, T. (2017). Membrane remodeling during embryonic abscission in Caenorhabditis elegans. J Cell Biol.
Lacroix, B., and Maddox, A.S. (2012). Cytokinesis, ploidy and aneuploidy. J Pathol *226*, 338-351.
Leung, B., Hermann, G.J., and Priess, J.R. (1999). Organogenesis of the Caenorhabditis elegans intestine. Dev Biol *216*, 114-134.
Li, D.Y., Mangan, A., Cicchini, L., Margolis, B., and Prekeris, R. (2014). FIP5 phosphorylation during mitosis regulates apical trafficking and lumenogenesis. Embo Rep *15*, 428-437.
Li, R. (2007). Cytokinesis in development and disease: variations on a common theme. Cell Mol Life Sci *64*, 3044-3058.
Linkert, M., Rueden, C.T., Allan, C., Burel, J.M., Moore, W., Patterson, A., Loranger, B., Moore, J., Neves, C., MacDonald, D.*, et al.* (2010). Metadata matters: access to image data in the real world. J Cell Biol *189*, 777-782.
Lujan, P., Varsano, G., Rubio, T., Hennrich, M.L., Sachsenheimer, T., Galvez-Santisteban, M., Martin-Belmonte, F., Gavin, A.C., Brugger, B., and Kohn, M. (2016). Phosphatase of regenerating liver (PRL)-3 disrupts epithelial architecture by altering the post-mitotic midbody position. J Cell Sci.
Maddox, A.S., Habermann, B., Desai, A., and Oegema, K. (2005). Distinct roles for two C-elegans anillins in the gonad and early embryo. Development *132*, 2837-2848.
Maddox, A.S., Lewellyn, L., Desai, A., and Oegema, K. (2007). Anillin and the septins promote asymmetric ingression of the cytokinetic furrow. Dev Cell *12*, 827-835.
Mathieu, J., Cauvin, C., Moch, C., Radford, S.J., Sampaio, P., Perdigoto, C.N., Schweisguth, F., Bardin, A.J., Sunkel, C.E., Mckim, K.*, et al.* (2013). Aurora B and Cyclin B Have Opposite Effects on the Timing of Cytokinesis Abscission in Drosophila Germ Cells and in Vertebrate Somatic Cells. Dev Cell *26*, 250-265.
McLachlan, I.G., and Heiman, M.G. (2013). Shaping dendrites with machinery borrowed from epithelia. Curr Opin Neurobiol *23*, 1005-1010.
McLean, P.F., and Cooley, L. (2013). Protein Equilibration Through Somatic Ring Canals in Drosophila. Science *340*, 1445-1447.
Morais-de-Sa, E., and Sunkel, C. (2013). Adherens junctions determine the apical position of the midbody during follicular epithelial cell division. Embo Rep *14*, 696-703.
Nechipurenko, I.V., Berciu, C., Sengupta, P., and Nicastro, D. (2017). Centriolar remodeling underlies basal body maturation during ciliogenesis in Caenorhabditis elegans. eLife *6*.
Norden, C., Mendoza, M., Dobbelaere, J., Kotwaliwale, C.V., Biggins, S., and Barral, Y. (2006). The NoCut pathway links completion of cytokinesis to spindle midzone function to prevent chromosome breakage. Cell *125*, 85-98.
Oegema, K., and Hyman, A.A. (2006). Cell division. WormBook : the online review of C elegans biology, 1-40.
Ou, G., Stuurman, N., D'Ambrosio, M., and Vale, R.D. (2010). Polarized myosin produces unequal-size daughters during asymmetric cell division. Science *330*, 677-680.
Ou, G.S., Gentili, C., and Gonczy, P. (2014). Stereotyped distribution of midbody remnants in early C. elegans embryos requires cell death genes and is dispensable for development. Cell Res *24*, 251-253.
Padmanabhan, A., and Zaidel-Bar, R. (2017). Non-junctional E-Cadherin Clusters Regulate the Actomyosin Cortex in the C. elegans Zygote. Mech Develop *145*, S85-S85.
Paolini, A., Duchemin, A.L., Albadri, S., Patzel, E., Bornhorst, D., Avalos, P.G., Lemke, S., Machate, A., Brand, M., Sel, S.*, et al.* (2015). Asymmetric inheritance of the apical domain and self-renewal of retinal ganglion cell progenitors depend on Anillin function. Development *142*, 832-839.
Perkins, L.A., Hedgecock, E.M., Thomson, J.N., and Culotti, J.G. (1986). Mutant Sensory Cilia in the Nematode Caenorhabditis-Elegans. Developmental Biology *117*, 456-487.

964 Pohl, C., and Bao, Z. (2010). Chiral forces organize left-right patterning in C. elegans by
965 uncoupling midline and anteroposterior axis. Dev Cell *19*, 402-412.
966 Pollarolo, G., Schulz, J.G., Munck, S., and Dotti, C.G. (2011). Cytokinesis remnants define
967 first neuronal asymmetry in vivo. Nat Neurosci *14*, 1525-1533.
968 Portereiko, M.F., Saam, J., and Mango, S.E. (2004). ZEN-4/MKLP1 is required to polarize
969 the foregut epithelium. Curr Biol *14*, 932-941.
970 Rasmussen, J.P., Feldman, J.L., Reddy, S.S., and Priess, J.R. (2013). Cell Interactions and
971 Patterned Intercalations Shape and Link Epithelial Tubes in C. elegans. Plos Genetics *9*.
972 Rasmussen, J.P., Reddy, S.S., and Priess, J.R. (2012). Laminin is required to orient epithelial
973 polarity in the C. elegans pharynx. Development *139*, 2050-2060.
974 Reinsch, S., and Karsenti, E. (1994). Orientation of Spindle Axis and Distribution of Plasma-
975 Membrane Proteins during Cell-Division in Polarized Mdckii Cells. J Cell Biol *126*, 1509-
976 1526.
977 Salzmann, V., Chen, C., Chiang, C.Y., Tiyaboonchai, A., Mayer, M., and Yamashita, Y.M.
978 (2014). Centrosome-dependent asymmetric inheritance of the midbody ring in Drosophila
979 germline stem cell division. Mol Biol Cell *25*, 267-275.
980 Sato, K., Norris, A., Sato, M., and Grant, B.D. (2014). C. elegans as a model for membrane
981 traffic. WormBook : the online review of C elegans biology, 1-47.
982 Schiel, J.A., Childs, C., and Prekeris, R. (2013). Endocytic transport and cytokinesis: from
983 regulation of the cytoskeleton to midbody inheritance. Trends Cell Biol *23*, 319-327.
984 Schiel, J.A., Park, K., Morphew, M.K., Reid, E., Hoenger, A., and Prekeris, R. (2011).
985 Endocytic membrane fusion and buckling-induced microtubule severing mediate cell
986 abscission. J Cell Sci *124*, 1411-1424.
987 Schindelin, J., Arganda-Carreras, I., Frise, E., Kaynig, V., Longair, M., Pietzsch, T., Preibisch,
988 S., Rueden, C., Saalfeld, S., Schmid, B.*, et al.* (2012). Fiji: an open-source platform for
989 biological-image analysis. Nat Methods *9*, 676-682.
990 Schluter, M.A., Pfarr, C.S., Pieczynski, J., Whiteman, E.L., Hurd, T.W., Fan, S.L., Liu, C.J.,
991 and Margolis, B. (2009). Trafficking of Crumbs3 during Cytokinesis Is Crucial for Lumen
992 Formation. Mol Biol Cell *20*, 4652-4663.
993 Schumacher, J.M., Golden, A., and Donovan, P.J. (1998). AIR-2: An Aurora/Ipl1-related
994 protein kinase associated with chromosomes and midbody microtubules is required for polar
995 body extrusion and cytokinesis in Caenorhabditis elegans embryos. J Cell Biol *143*, 1635-
996 1646.
997 Severson, A.F., Hamill, D.R., Carter, J.C., Schumacher, J., and Bowerman, B. (2000). The
998 Aurora-related kinase AIR-2 recruits ZEN-4/CeMKLP1 to the mitotic spindle at metaphase
999 and is required for cytokinesis. Curr Biol *10*, 1162-1171.
1000 Siller, K.H., and Doe, C.Q. (2009). Spindle orientation during asymmetric cell division. Nat
1001 Cell Biol *11*, 365-374.
1002 Singh, D., and Pohl, C. (2014). Coupling of Rotational Cortical Flow, Asymmetric Midbody
1003 Positioning, and Spindle Rotation Mediates Dorsoventral Axis Formation in C. elegans. Dev
1004 Cell *28*, 253-267.
1005 Skop, A.R., Liu, H., Yates, J., 3rd, Meyer, B.J., and Heald, R. (2004). Dissection of the
1006 mammalian midbody proteome reveals conserved cytokinesis mechanisms. Science *305*, 61-
1007 66.
1008 Smith, K.P., Kieserman, E.K., Wang, P.I., Basten, S.G., Giles, R.H., Marcotte, E.M., and
1009 Wallingford, J.B. (2011). A Role for Central Spindle Proteins in Cilia Structure and Function.
1010 Cytoskeleton *68*, 112-124.
1011 Steigemann, P., Wurzenberger, C., Schmitz, M.H.A., Held, M., Guizetti, J., Maar, S., and
1012 Gerlich, D.W. (2009). Aurora B-Mediated Abscission Checkpoint Protects against
1013 Tetraploidization. Cell *136*, 473-484.
1014 Sulston, J.E., Schierenberg, E., White, J.G., and Thomson, J.N. (1983). The embryonic cell
1015 lineage of the nematode Caenorhabditis elegans. Dev Biol *100*, 64-119.
1016 Tong, Y.G., and Burglin, T.R. (2010). Conditions for dye-filling of sensory neurons in
1017 Caenorhabditis elegans. J Neurosci Meth *188*, 58-61.

1018 van Furden, D., Johnson, K., Segbert, C., and Bossinger, O. (2004). The C-elegans ezrin-
1019 radixin-moesin protein ERM-1 is necessary for apical junction remodelling and tubulogenesis
1020 in the intestine. Developmental Biology *272*, 262-276.
1021 Von Stetina, S.E., Liang, J., Marnellos, G., and Mango, S.E. (2017). Temporal regulation of
1022 epithelium formation mediated by FoxA, MKLP1, MgcRacGAP, and PAR-6. Mol Biol Cell
1023 *28*, 2042-2065.
1024 Waddle, J.A., Cooper, J.A., and Waterston, R.H. (1994). Transient localized accumulation of
1025 actin in Caenorhabditis elegans blastomeres with oriented asymmetric divisions.
1026 Development *120*, 2317-2328.
1027 Wang, J., Silva, M., Haas, L.A., Morsci, N.S., Nguyen, K.C.Q., Hall, D.H., and Barr, M.M.
1028 (2014a). C-elegans Ciliated Sensory Neurons Release Extracellular Vesicles that Function in
1029 Animal Communication. Curr Biol *24*, 519-525.
1030 Wang, T., Yanger, K., Stanger, B.Z., Cassio, D., and Bi, E. (2014b). Cytokinesis defines a
1031 spatial landmark for hepatocyte polarization and apical lumen formation. Journal of Cell
1032 Science *127*, 2483-2492.
1033 Wilcock, A.C., Swedlow, J.R., and Storey, K.G. (2007). Mitotic spindle orientation
1034 distinguishes stem cell and terminal modes of neuron production in the early spinal cord.
1035 Development *134*, 1943-1954.
1036 Yang, R.Z., and Feldman, J.L. (2015). SPD-2/CEP192 and CDK Are Limiting for
1037 Microtubule-Organizing Center Function at the Centrosome. Curr Biol *25*, 1924-1931.
1038 Zenker, J., White, M.D., Templin, R.M., Parton, R.G., Thorn-Seshold, O., Bissiere, S., and
1039 Plachta, N. (2017). A microtubule-organizing center directing intracellular transport in the
1040 early mouse embryo. Science *357*, 925-+.

Figure 1

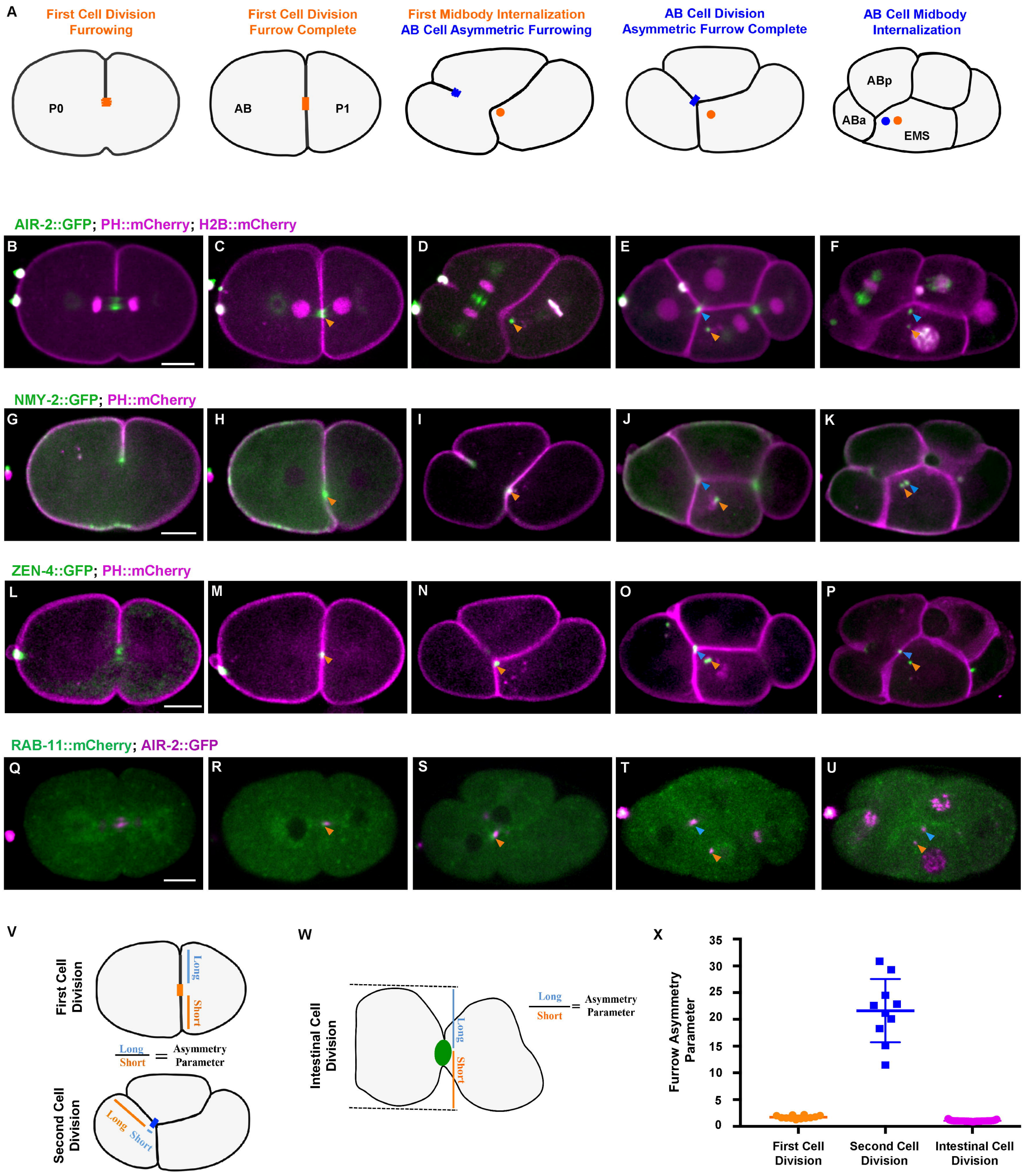
A
First Cell Division Furrowing
First Cell Division Furrow Complete
First Midbody Internalization AB Cell Asymmetric Furrowing
AB Cell Division Asymmetric Furrow Complete
AB Cell Midbody Internalization
P0
AB
P1
ABp
ABa
EMS
AIR-2::GFP; PH::mCherry; H2B::mCherry
B
C
D
E
F
NMY-2::GFP; PH::mCherry
G
H
I
J
K
ZEN-4::GFP; PH::mCherry
L
M
N
O
P
RAB-11::mCherry; AIR-2::GFP
Q
R
S
T
U
V
First Cell Division
Long
Short
Long / Short = Asymmetry Parameter
Second Cell Division
Long
Short
W
Intestinal Cell Division
Long
Short
Long / Short = Asymmetry Parameter
X
Furrow Asymmetry Parameter
35
30
25
20
15
10
5
0
First Cell Division
Second Cell Division
Intestinal Cell Division

Figure 2

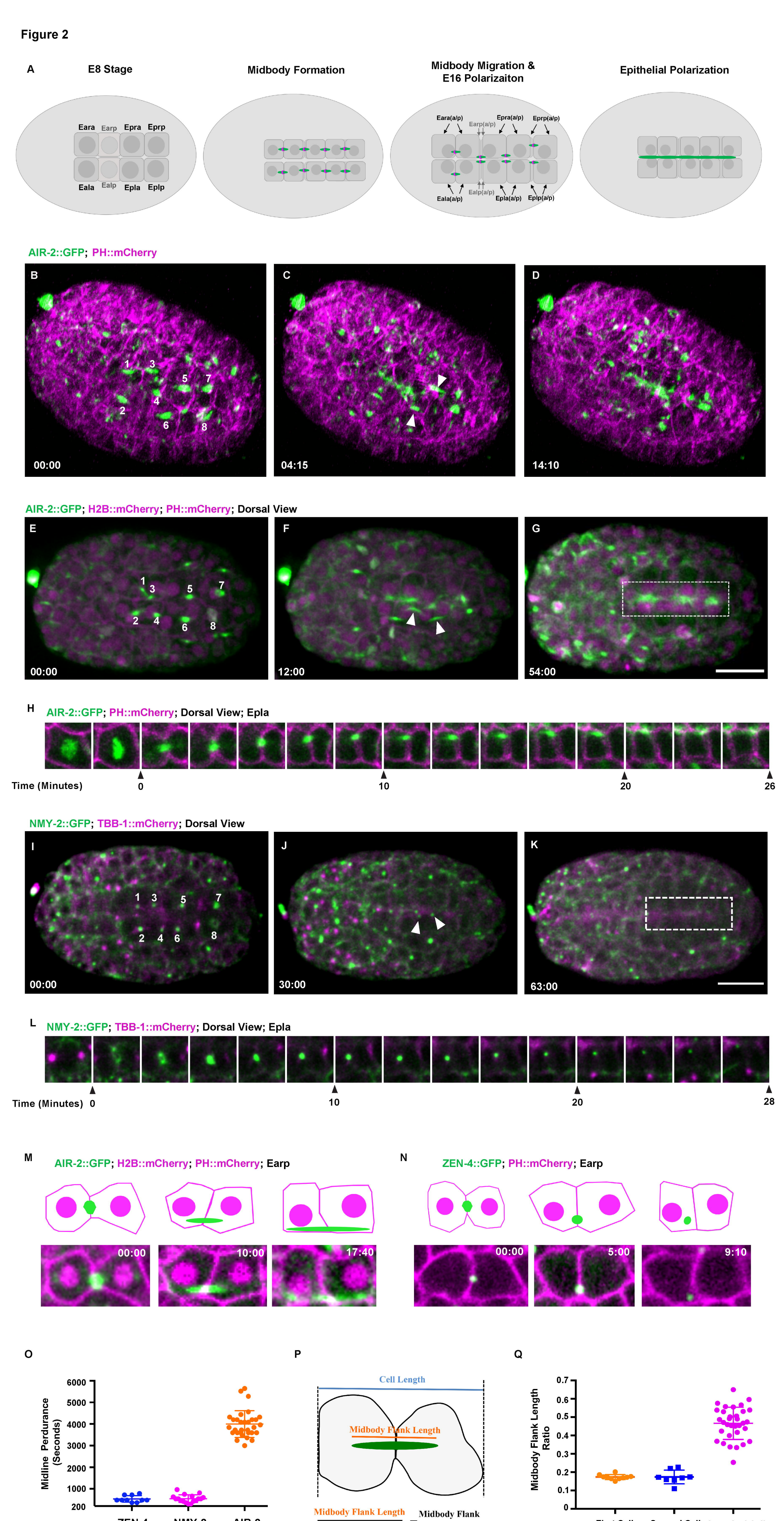
A
E8 Stage
Midbody Formation
Midbody Migration & E16 Polarizaiton
Epithelial Polarization
Eara
Earp
Epra
Eprp
Eala
Ealp
Epla
Eplp
Eara(a/p)
Earp(a/p)
Epra(a/p)
Eprp(a/p)
Ealp(a/p)
Eala(a/p)
Epla(a/p)
Eplp(a/p)
AIR-2::GFP; PH::mCherry
B
C
D
00:00
04:15
14:10
AIR-2::GFP; H2B::mCherry; PH::mCherry; Dorsal View
E
F
G
00:00
12:00
54:00
H
AIR-2::GFP; PH::mCherry; Dorsal View; Epla
Time (Minutes)
0
10
20
26
NMY-2::GFP; TBB-1::mCherry; Dorsal View
I
J
K
00:00
30:00
63:00
L
NMY-2::GFP; TBB-1::mCherry; Dorsal View; Epla
Time (Minutes)
0
10
20
28
M
AIR-2::GFP; H2B::mCherry; PH::mCherry; Earp
00:00
10:00
17:40
N
ZEN-4::GFP; PH::mCherry; Earp
00:00
5:00
9:10
O
Midline Perdurance (Seconds)
6000
5000
4000
3000
2000
1000
200
ZEN-4
NMY-2
AIR-2
P
Cell Length
Midbody Flank Length
Midbody Flank Length / Cell Length = Midbody Flank Ratio
Q
Midbody Flank Length Ratio
0.7
0.6
0.5
0.4
0.3
0.2
0.1
0
First Cell Division
Second Cell Division
Intestinal Cell Division

Figure 3

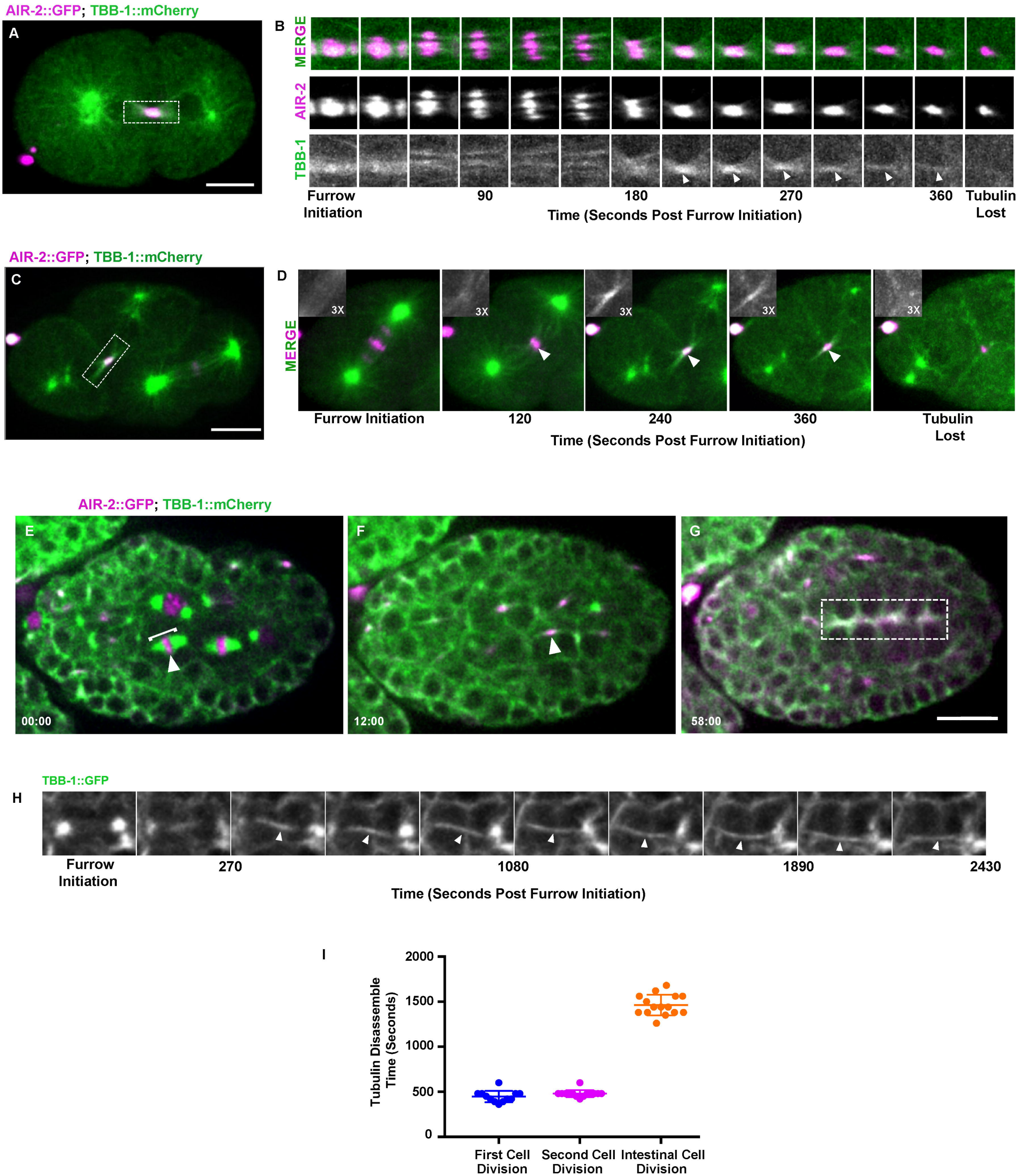
AIR-2::GFP; TBB-1::mCherry
A
B
MERGE
AIR-2
TBB-1
Furrow Initiation
90
180
270
360
Tubulin Lost
Time (Seconds Post Furrow Initiation)
AIR-2::GFP; TBB-1::mCherry
C
D
MERGE
3X
Furrow Initiation
120
240
360
Tubulin Lost
Time (Seconds Post Furrow Initiation)
AIR-2::GFP; TBB-1::mCherry
E
F
G
00:00
12:00
58:00
TBB-1::GFP
H
Furrow Initiation
270
1080
1890
2430
Time (Seconds Post Furrow Initiation)
I
Tubulin Disassemble Time (Seconds)
2000
1500
1000
500
0
First Cell Division
Second Cell Division
Intestinal Cell Division

Figure 4

A

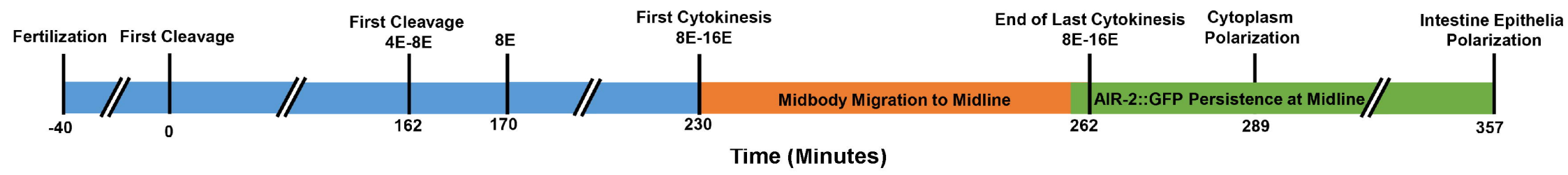

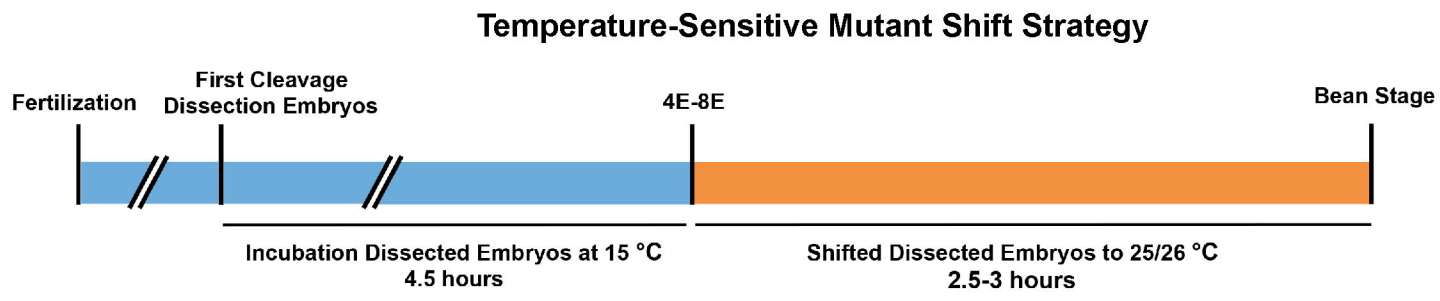

B

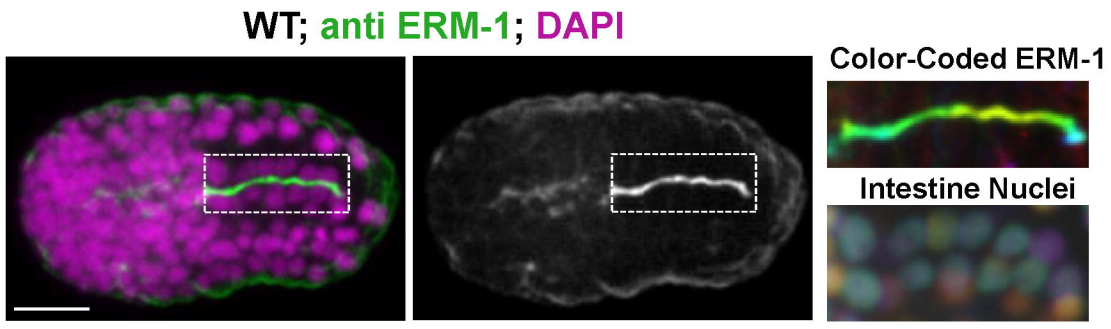

C *air-2 (or207ts);* anti ERM-1; DAPI

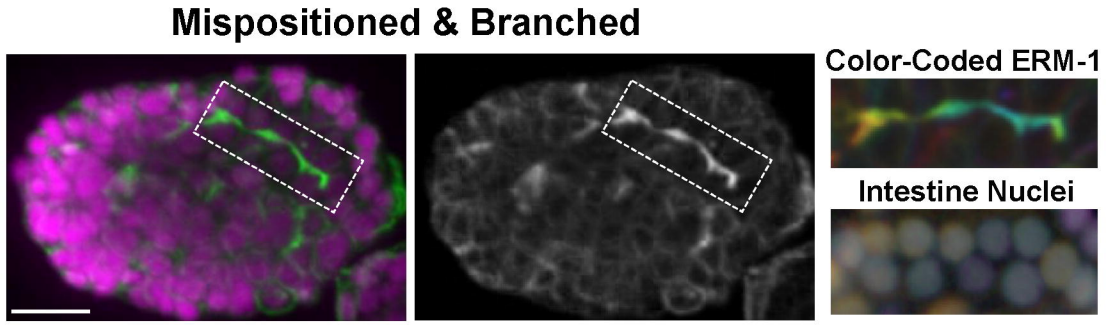

D *air-2 (or207ts);* anti ERM-1; DAPI

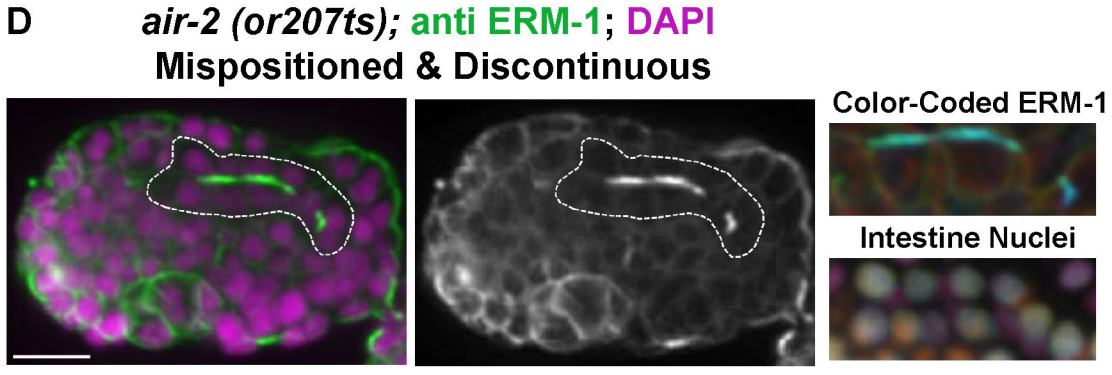

E *air-2 (or207ts);* anti ERM-1; DAPI

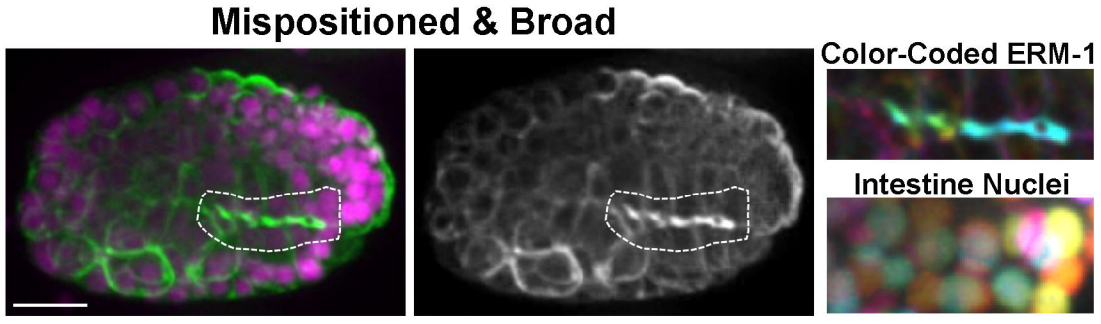

F *zen-4 (or153ts);* anti ERM-1; DAPI

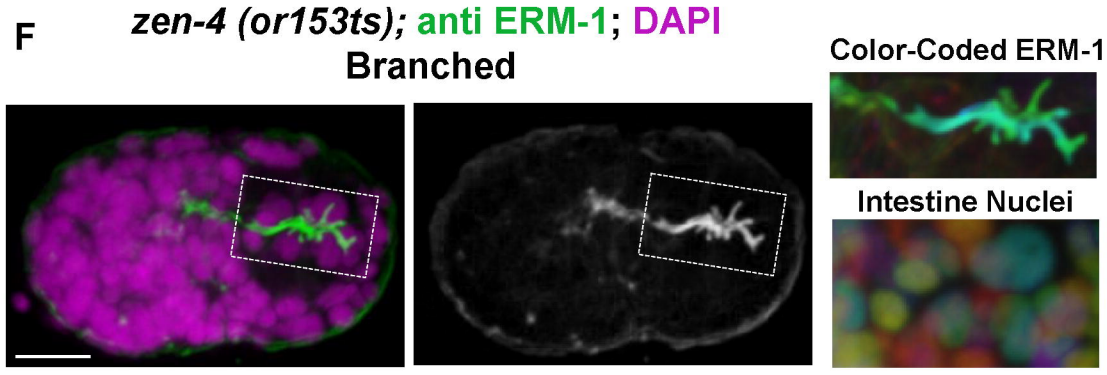

G *spd-1 (oj5ts);* anti ERM-1; DAPI

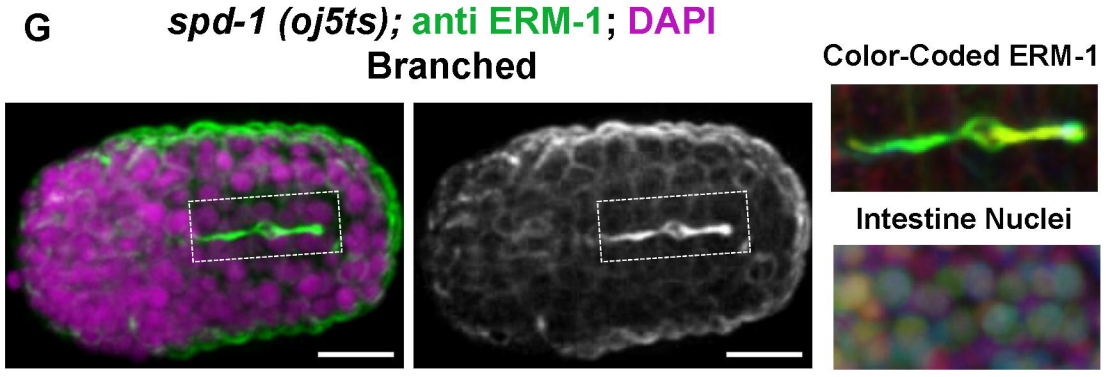

H

	Mispositioned	Discontinuous	Broad	Branched
WT (N2)	0% (0/60)	0% (0/60)	3.3% (2/60)	20% (12/60)
air-2 (or207ts)	60.9% (25/41)	43.9% (18/41)	12.1% (5/41)	65.9% (27/41)
zen-4 (or153ts)	27.3% (6/22)	27.3% (6/22)	81.8% (18/22)	81.8% (18/22)
spd-1 (oj5ts)	0% (0/59)	28.8% (17/59)	10.2% (6/59)	40% (24/59)

I

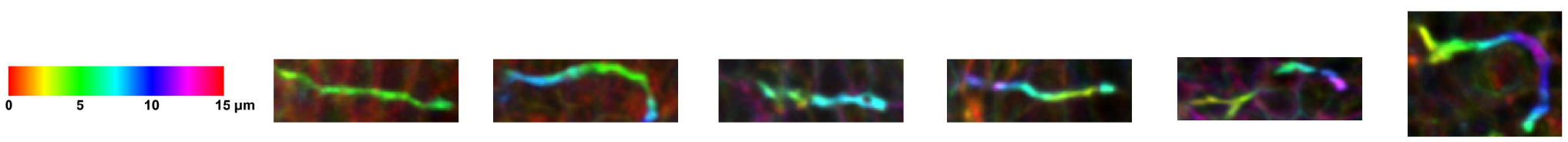

	One Color	Two Color	Three Color	Four Color	Five Color	Six Color
WT (N2)	25% (15/60)	40% (24/60)	31.7% (19/60)	3.3% (2/60)	0% (0/60)	0% (0/60)
air-2 (or207ts)	0% (0/41)	22.0% (9/41)	12.2% (9/41)	34.1% (14/41)	14.6% (6/41)	17.1% (7/41)
zen-4 (or153ts)	0% (0/22)	27.3% (6/22)	40.9% (9/22)	22.7% (5/22)	4.5% (1/22)	0% (0/22)
spd-1 (oj5ts)	10.2% (6/59)	55.9% (33/59)	27.1% (16/59)	1.7% (1/59)	1.7% (1/59)	0% (0/59)

Figure 5

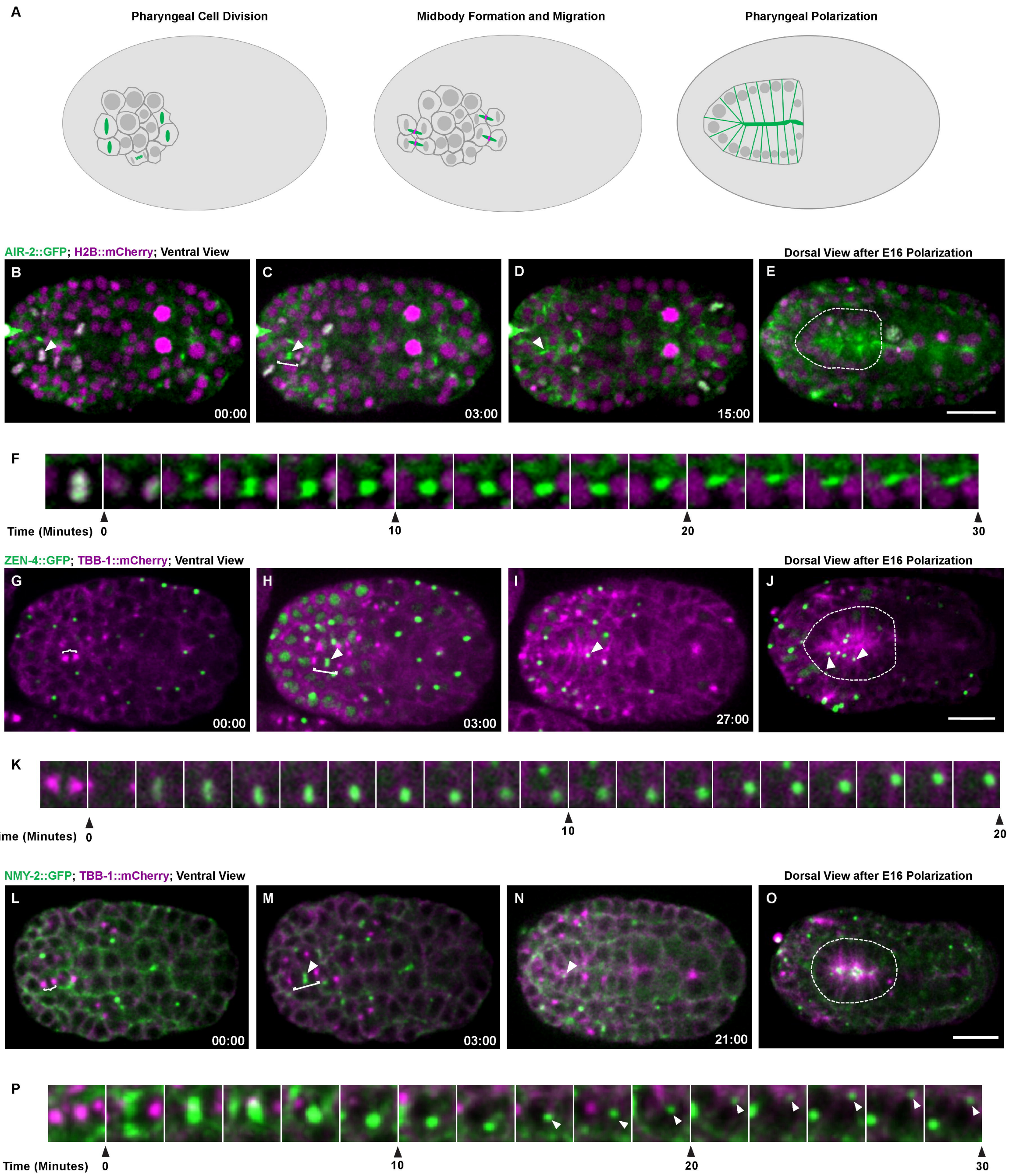
A
Pharyngeal Cell Division
Midbody Formation and Migration
Pharyngeal Polarization
AIR-2::GFP; H2B::mCherry; Ventral View
Dorsal View after E16 Polarization
B
00:00
C
03:00
D
15:00
E
F
Time (Minutes) 0
10
20
30
ZEN-4::GFP; TBB-1::mCherry; Ventral View
Dorsal View after E16 Polarization
G
00:00
H
03:00
I
27:00
J
K
Time (Minutes) 0
10
20
NMY-2::GFP; TBB-1::mCherry; Ventral View
Dorsal View after E16 Polarization
L
00:00
M
03:00
N
21:00
O
P
Time (Minutes) 0
10
20
30

Figure 6

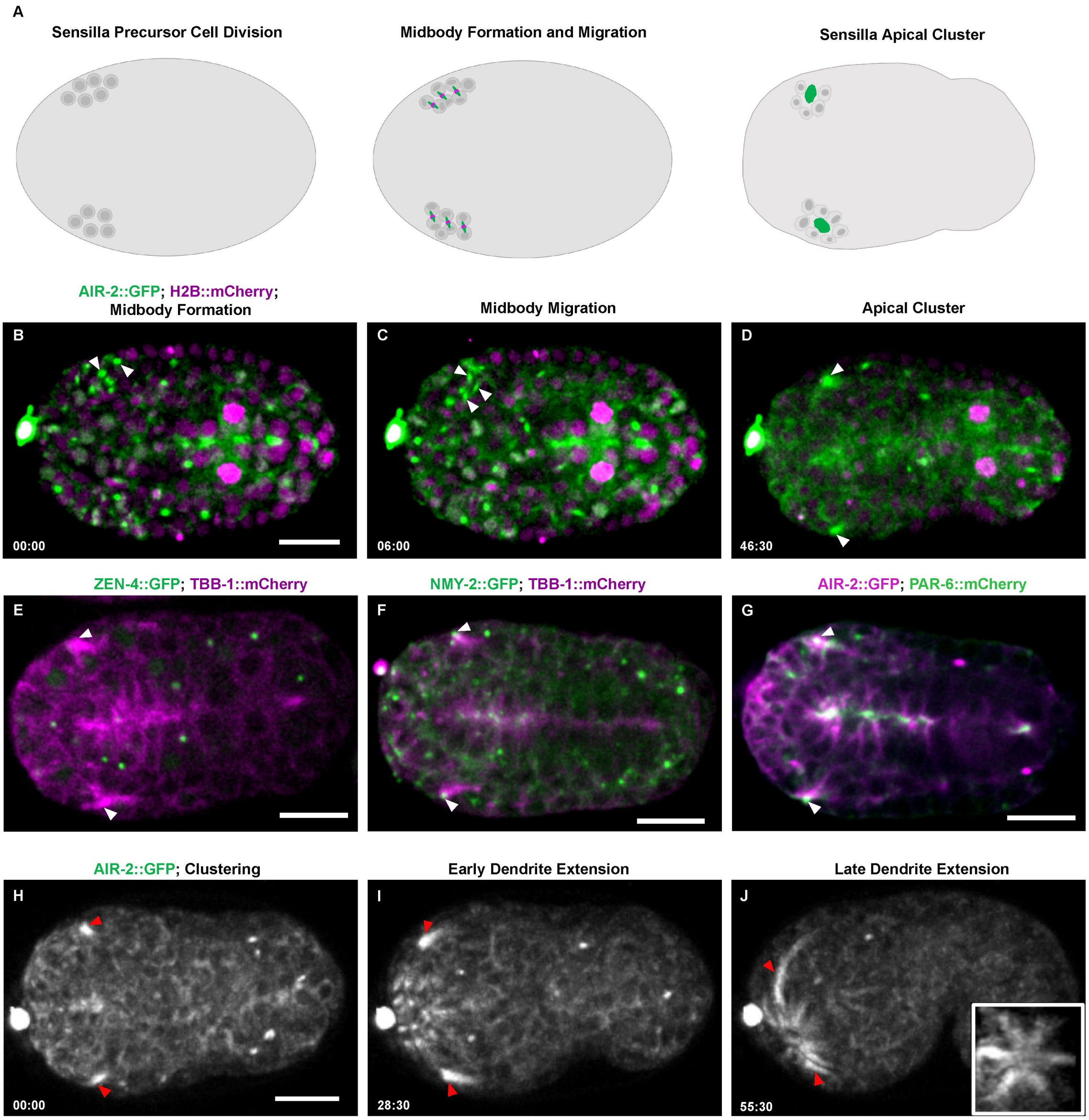
A
Sensilla Precursor Cell Division
Midbody Formation and Migration
Sensilla Apical Cluster
AIR-2::GFP; H2B::mCherry;
Midbody Formation
Midbody Migration
Apical Cluster
B
C
D
00:00
06:00
46:30
ZEN-4::GFP; TBB-1::mCherry
NMY-2::GFP; TBB-1::mCherry
AIR-2::GFP; PAR-6::mCherry
E
F
G
AIR-2::GFP; Clustering
Early Dendrite Extension
Late Dendrite Extension
H
I
J
00:00
28:30
55:30

Figure 7

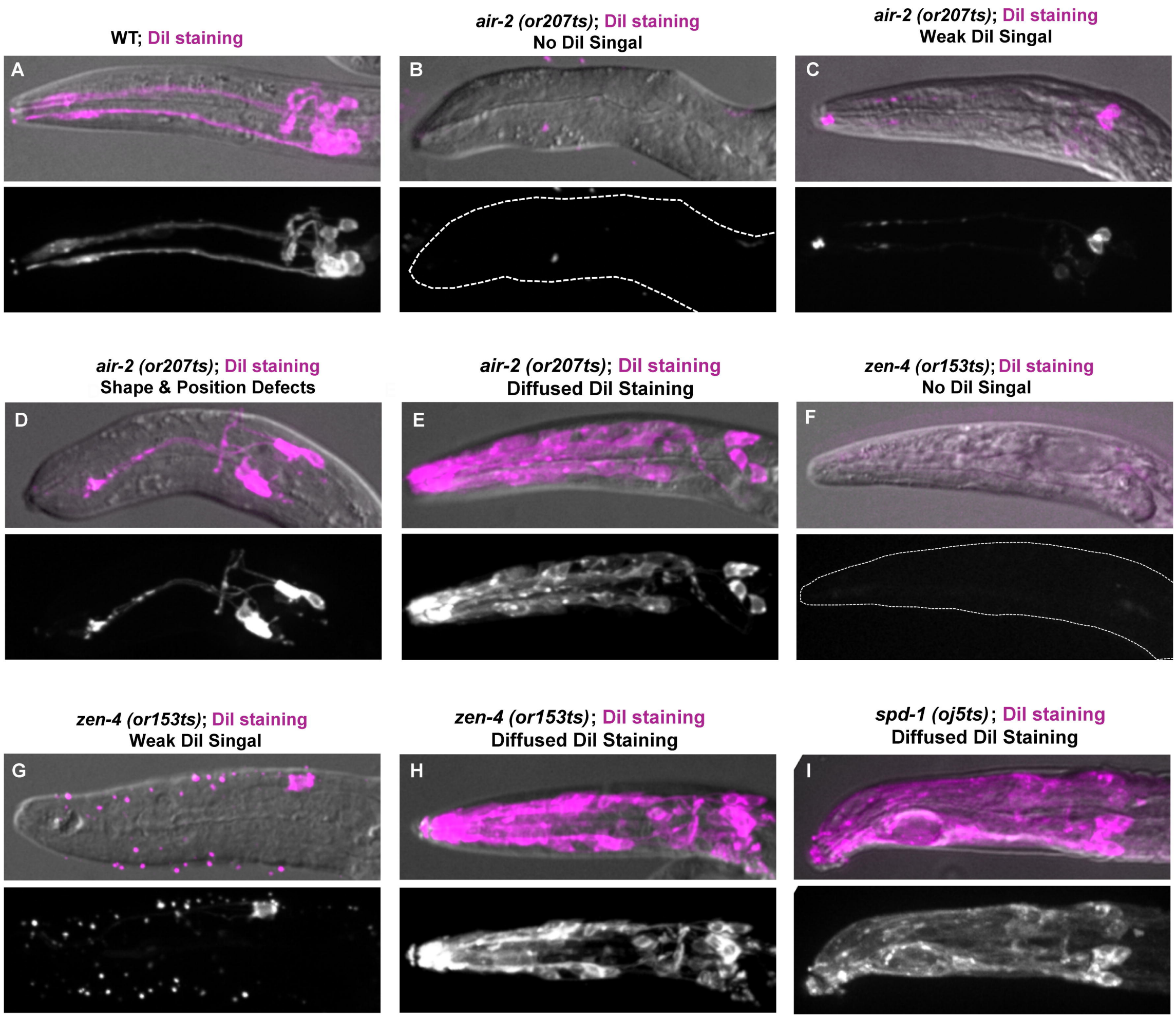
WT; Dil staining
A
air-2 (or207ts); Dil staining
No Dil Singal
B
air-2 (or207ts); Dil staining
Weak Dil Singal
C
air-2 (or207ts); Dil staining
Shape & Position Defects
D
air-2 (or207ts); Dil staining
Diffused Dil Staining
E
zen-4 (or153ts); Dil staining
No Dil Singal
F
zen-4 (or153ts); Dil staining
Weak Dil Singal
G
zen-4 (or153ts); Dil staining
Diffused Dil Staining
H
spd-1 (oj5ts); Dil staining
Diffused Dil Staining
I